Ionic-Complementary Peptide Modified Electrode for Biosensing Application

by

Zhenyu Qian

A thesis

presented to the University of Waterloo

in fulfillment of the

thesis requirement for the degree of

Master of Applied Science

in

Chemical Engineering

Waterloo, Ontario, Canada, 2009

AUTHOR'S DECLARATION

I hereby declare that I am the sole author of this thesis. This is a true copy of the thesis, including any required final revisions, as accepted by my examiners.

I understand that my thesis may be electronically available to the public.

Zhenyu Qian

Abstract

Self-assembling peptides have emerged as new nanobiomaterials and received considerable attention in the areas of nanoscience and biomedical engineering. One important type is the ionic-complementary peptide, which contains special patterns of positive and negative charge distribution. This thesis explores the application of this special type of peptides for the modification of electrode surfaces. The ionic-complementary peptide modified electrode was then further used to immobilize biologically active molecules, glucose oxidase in the present case, to construct a biosensor. There are two major parts in this thesis.

In the first part, an ionic-complementary peptide, EFK16-II, was used to modify a highly ordered pyrolytic graphite (HOPG) electrode surface. The nanofibre structure of the self-assembling peptide on the electrode surface was characterized by atomic force microscopy (AFM). Attenuated total reflection fourier transform infrared sectroscopy (ATR-FTIR) spectra showed that upon addition of 1-ethyl-3-(3-dimethylaminopropyl) carbodiimide (EDC), EFK16-II molecules tend to be cross-linked among themselves. Cross-linking of the peptide diminishes the number of carboxyl groups available for immobilizing a sensing enzyme, i.e., glucose oxidase (GOx). A simple method based on pre-mixing the carbodiimide and GOx was developed; it inhibited peptide cross-linking and significantly improved enzyme immobilization. Biosensors constructed in this way showed increased overall signal intensity and a much higher sensitivity at 4.94mA M^{-1} cm^{-2}, a six-fold increase compared to the previously-reported peptide-modified electrodes.

In the second part, another ionic-complementary peptide, EAK16-II, was used to modify the HOPG electrode. AFM images showed that EAK16-II formed well-ordered nanofibre patterns on

the electrode surface. The redox couple $Fe(CN)_6^{3-/4-}$ was used as a probe to detect the electrochemical properties of the EAK16-II modified electrode. The results showed that the electron transfer at the electrode surface does not change much before and after modification. GOx was immobilized onto the EAK16-II modified HOPG and showed a good response to the concentration change of glucose. Similar to the EFK16-II, inter- or intro-peptide cross-linking also occurs when the solution containing EDC and sulfo-NHS was injected onto EAK16-II modified electrode. The same method as in the first part was applied here to prevent peptide cross-linking. The sensitivity was improved from 0.53mA $M^{-1}cm^{-2}$ to 2.4mA $M^{-1}cm^{-2}$.

A proposal for constructing a reagentless biosensor by immobilizing both enzyme and mediator onto the electrode was made. However, the results indicated that the mediator, ferrocene carboxylic acid (FCA), was not stable on the surface after being immobilized. A redox protein, cytochrome *c* (Cyt *c*), was also immobilized onto an EAK16-II modified electrode. Direct electron transfer (DET) between the redox center of Cyt *c* and the electrode was observed. However, cyclic voltammetry results indicated that the peptide did not help improve the DET of modified Cyt *c*.

The results presented here demonstrate significant potential for ionic-complementary peptides for constructing electrochemical biosensors.

Acknowledgements

First of all, I would like to express my deepest gratitude to my supervisor, Professor Pu Chen, for his endless guidance and help during my master's study. I thank him for giving me financial support and the opportunity of doing this cutting edge research. He imparted me the critical thinking and scientific methods of doing research. Without his sustained encouragement and support, I could not finish my master's degree successfully. I am sure that what I learned during this two years' period will benefit me tremendously for the rest of my life.

I also want to thank Professor Susan Mikkelsen for letting me do electrochemical experiment in her lab and her insightful suggestions for my project. I would like to give my special thanks to Dr. Hong Yang. She gave me the fundamental knowledge in biosensor and solid training in operating experimental apparatus. I thank Professor H. Tao for his suggestions of extending my work in protein immobilization.

I also want to extend my thanks to everyone in the bio-nano engineering research group, Ibrahim Hassan, Hamid Firooz, Parisa Sadatmousavi, Mousa Jafari, Madjid Soltani, Hua Wei, Hui Wang, Bahram Zargar and Yuebiao Sheng for their encouragement and friendship. I also thank undergraduate research assistants Mikhail and Mushfique for helping me doing experiment.

Last, my greatest gratitude to my family. They supported me all the time whatever happened to me. Without their unlimited love, understanding and support, none of my achievement would be possible.

Table of Contents

List of Figures

List of Tables

Chapter 1 Introduction

1.1 Overview

Sensors are defined as devices that measure a physical quantity and convert it into a signal which can be read by an observer or by an instrument. Sensors exist all round the world, not only in technical and research fields, but also in our daily life. For example, a mercury thermometer is a sensor because the temperature causes the expansion and contraction of a liquid which can be read on a calibrated glass tube.

Rapid, reliable, inexpensive, and in some cases, continuous measurement of analytes has been the major goal in analytical sciences. Since biosensors offer many advantages over conventional analytical techniques, the development of biosensors for analytical purposes has attracted a great deal of interest in recent years. By definition, biosensors are analytical devices that combine a biologically sensitive element (bio-recognition agent) with a physical or chemical transducer (e.g., a noble metal or graphite electrode, optical fibers, surface acoustic wave or calorimetric devices) to selectively detect and measure the amount of specific compounds in a given external environment[1]. The bio-recognition agent is a bioactive substance, e.g., enzyme, antibody and micro-organism. These substances are capable of recognizing their specific analytes and also regulate the specificity and sensitivity of the device.

One of the advantages of biosensors is that they are highly selective. This is because the bio-recognition agent is capable of recognizing a specific substrate and transferring concentration information of the substrate to the transducer. Biosensors offer the possibility of real-time analysis, important for the rapid measurement of body analytes. The application of biosensors usually lies in the clinical analysis for health care.

The key element in the design of a suitable sensor architecture is the immobilization of a specific bio-recognition agent such as an enzyme on the transducer surface[2]. For this purpose, suitable surface linkers or matrices are therefore required to immobilize the enzyme on the surface and provide a biocompatible platform to allow the enzyme to function properly and effectively. The unique properties of the ionic-complementary peptides make them good candidates in biosensing application. First, these peptides usually have amphiphilic property, with both hydrophobic and hydrophilic parts in the molecular structure. Since most carbon-based electrodes are hydrophobic, the peptides have good affinity toward the electrode surface so that the electrodes can be modified by the peptides. Second, unlike other organic/inorganic materials, peptides consist of amino acids, which are contained in enzymes. Compared to organic/inorganic material modified surfaces, the peptide modified surfaces are more likely to be biocompatible and help maintain the bioactivity of the enzymes. Third, the ionic-complementary peptides follow some specific patterns and different peptides can easily be designed just by substituting the amino acid with another one having similar property. For example, the hydrophobic residues of the peptide can be substituted by other hydrophobic amino acids.

The main purpose of this study is to explore the application of ionic-complementary peptides in biomolecular sensing. Two typical ionic-complementary peptides, EAK16-II and EFK16-II, which contain the hydrophobic residues alanine (A) and phenylalanine (F), respectively, have been chosen for this study. These peptides also contain hydrophilic residues, glutamic acid (E) and lysine (K), which provide functional groups for enzyme immobilization.

1.2 Research Objectives

The objectives of this study are to:

1. use the ionic-complementary peptide EFK16-II to construct a glucose biosensor;
2. study the mechanism of the immobilization of the enzyme glucose oxidase (GOx) and methods to improve the signal intensity of the glucose biosensor;
3. study the properties of the EAK16-II-modified HOPG electrode and explore its application in glucose concentration detection;
4. study the immobilization of cytochrome *c* on the EAK16-II-modified electrode and its direct electron transfer on the electrode.

Chapter 2 Literature Review

2.1 Definition and Classification of Biosensors

2.1.1 Definition of Biosensors

A chemical sensor is a device that transforms chemical information, ranging from the concentration of a specific sample component to total composition analysis, into an analytically useful signal. Chemical sensors consist of two major parts: a chemical recognition system (receptor) and a physico-chemical transducer. Biosensors are chemical sensors in which the recognition system utilizes a biochemical mechanism.[3,4] Figure 2.1 shows the general configuration of a biosensor. The biological recognition system translates information from the biochemical domain into a chemical or physical output signal with a high degree of selectivity. The transducer converts this chemical or physical signal into a measurable electronic signal.[5] Since biosensors offer many advantages over conventional analytical techniques in terms of simplicity, detection limit, specificity and sensitivity, the development of biosensors for analytical purposes has attracted significant interest in recent years. Biosensors have widespread applications in medical analysis, environmental monitoring and industrial process control.[6-8]

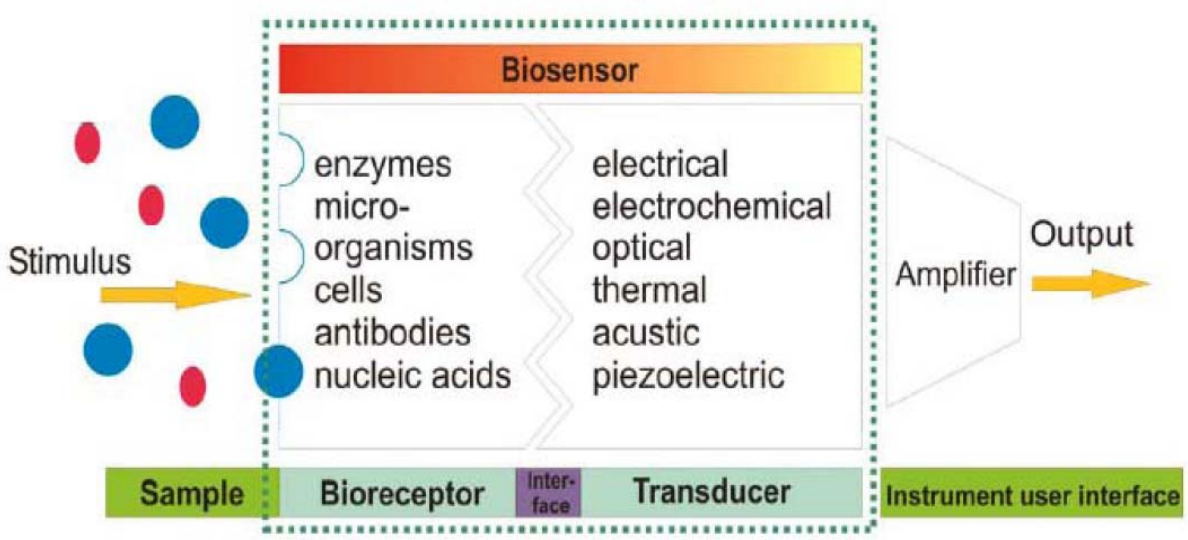

Figure 2.1 Schematic architecture of a biosensor

2.1.2 Classification of Biosensors

Based on the types of transducer used, biosensors have been divided into optical, calorimetric, piezoelectric and electrochemical biosensors.

2.1.2.1 Optical Biosensors

Optical biosensors are based on the measurement of light absorbed or emitted as a consequence of a biochemical reaction.[9,10] One of the major advantages of optical sensors is their ability to probe surfaces and films in a non-destructive manner. Additionally, they offer advantages in speed, safety, sensitivity and robustness, as well as permitting *in situ* sensing and real-time measurements. Optical immunosensors are currently receiving attention as alternatives to conventional immunoassay techniques because of the promise of enhanced sensitivity and the elimination of expensive, complex and time-consuming separation and incubation procedures. An optical immunosensor consists of either an antibody or antigen immobilized on a suitable surface.

The primary function of this type of sensor is to produce a measurable signal (which can be followed optically) upon interaction with a biospecific immunological component. The signal amplitude is related to the amount of antibody, antigen or hapten present in the sample.[11-13] However, optical biosensors are very sensitive and they cannot be used in turbid media.

2.1.2.2 Calorimetric Biosensors

Calorimetric biosensors detect an analyte on the basis of the heat evolved due to the biochemical reaction of the analyte with a suitable enzyme. Recently, integrated circuit temperature-sensitive structures have been modified with enzymes. Different substrates, enzymes, vitamins and antigens have been detected using thermometric biosensors. The most commonly used approach in the thermal enzyme probes is related to the enzyme directly attached to the thermistor.[14,15] Calorimetric biosensors are not widely used, primarily because most of the heat evolved in the biochemical reaction is lost to the surroundings without being detected, leaving the sensor with a low sensitivity.

2.1.2.3 Piezoelectric Biosensors

Piezoelectric biosensors operate on the principle of generation of electric dipoles on subjecting an anisotropic natural crystal to mechanical stress. Adsorption of the analyte increases the mass of the crystal and alters its basic frequency of oscillation. The use of piezoelectric transducers in biosensors was foreshadowed in the work of Sauerbrey who not only pioneered the use of the quartz crystal microbalance (QCM) but thoroughly analyzed the physics of the device.[16] The concept was then extended to chemical sensing by applying suitable sorption detection coatings to a QCM to selectively detect gases[17] and antibodies.[18] Nowadays, many

other biological species such as ammonia, nitrous oxide, methane and certain organophosphorus compounds[19,20] can be detected by piezoelectric biosensors.

2.1.2.4 Electrochemical Biosensors

Electrochemical biosensors are the most commonly used class of biosensors. These are based on the fact that during many bio-interaction processes, electrons are consumed or generated producing an electrochemical signal which can in turn be measured by an electrochemical detector. Electrochemical biosensors are favored over optical sensors mainly because of cost and availability, while thermal biosensors can not be used in turbid media.[21] Electrochemical biosensors can be operated in turbid media, have comparable instrumental sensitivity and are more amenable to miniaturization. Based on the electrochemical property that is measured by the detector system, electrochemical biosensors can be divided into conductometric, potentiometric and amperometric biosensors.

Conductometric biosensors measure the changes in the conductance between a pair of metal electrodes as a consequence of the biological component. Potentiometric biosensors measure potentials at the working electrode with respect to the reference electrode when zero or no significant current follows between them.[22-24] For potentiometric measurements, the relationship between concentration and the potential is governed by the Nernst equation. Potentiometric sensors offer low detection limits for various ions such as Na^+, K^+, Ca^{2+}, H^+ and NH_4^+ and usually have no chemical influence on samples.

Amperometric biosensors measure the changes in the current passed by the working electrode due to the oxidation or reduction of the analyte on the electrode surface. The oldest bioanalytical application of amperometry is the measurement of dissolved oxygen concentration. It exploits a

gas-permeable membrane for selectivity, across which oxygen diffuses and is reduced at the electrode at a constant potential.[25] The most important category of amperometric biosensors includes enzyme-based biosensors. The first enzyme biosensor was reported by Clark[26] in 1962. This biosensor consists of glucose oxidase bound to a membrane covering an amperometric oxygen electrode. This was the first device that could be used to measure the concentration of an enzyme substrate without adding an enzyme as a reagent to the analyte solution. However, the oxidase-based devices rely on the use of oxygen as the physiological electron acceptor and are subject to errors due to fluctuations in the oxygen activity. Artificial electron acceptor known as a mediator is introduced as a substitute for oxygen and shuttles electrons from enzyme to the electrode. Ferrocene and its derivatives, ferricyanide, methylene blue, benzoquinone and N-methyl phenazine etc. are the most commonly used mediators in biosensors.[27-31] In addition, the application of mediator also allows the enzyme electrode to operate at a lower potential so that some interferences such as ascorbic acid, uric acid and acetaminophen are not electroactive.[32]

2.2 Materials Used for Electrode Modification

Electrochemical biosensors have emerged as the most commonly used biosensors. One typical kind of electrochemical biosensor utilizes enzyme-modified electrodes. The general configuration of an enzyme-based amperometric biosensor comprises an immobilized enzyme as the chemically selective layer, an electrode as transducer that is coupled to an amplifier, processor and the display[33,34] as shown in Figure 2.2.

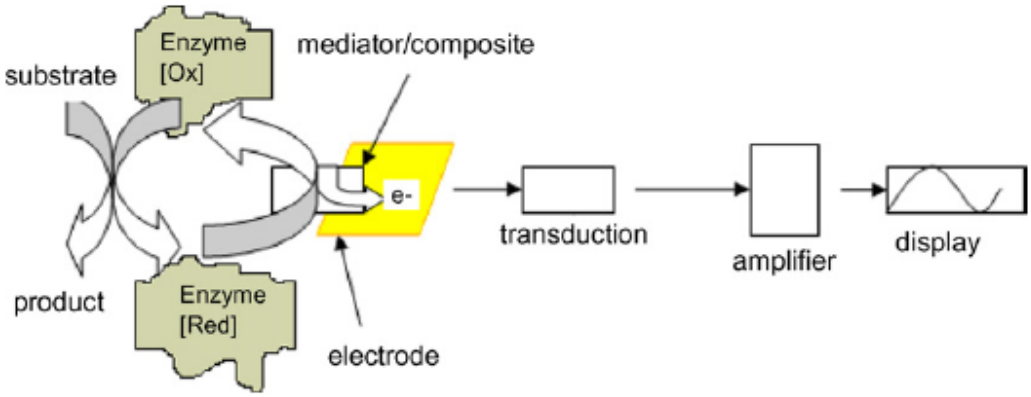

Figure 2.2 Basic elements of an enzymatic biosensor[35]

The immobilization of the enzymes on the electrode surface is considered as one of the most critical steps that dictates the effectiveness of these electrodes. Different chemical, biochemical or physical techniques, e.g., chemical crosslinking with glutaraldehyde or other bifunctinal agents,[36,37] antigen-antibody interactions (e.g. based on avidin biotin binding),[38] magnetic interactions,[39,40] entrapment or encapsulation within polymers[41] and the formation of pasted materials[42] have been exploited for this purpose.

2.2.1 Self-assembled Monolayers (SAMs)

A self-assembled monolayer (SAM) is formed by the strong chemisorption between the substrate and head group of selected organic molecule.[43,44] SAM provides one simple route to functionalize electrode surfaces by organic molecules (both aliphatic and aromatic) containing free anchor groups such as thiols, disulphides, amines, silanes or acids. The best characterized systems of SAMs are alkanethiolates $X(CH_2)_nS^-$ on gold.[45,46] The formation of such a SAM is

shown in Figure 2.3.[47] The sulfur atoms form a commensurate overlayer on Au (111) with a tilting degree of 30°. The thickness of the monolayer is determined by the number of methylene groups (n) in the alkyl chain. The surface properties of the monolayer can be easily modified by changing the head group X.[48]

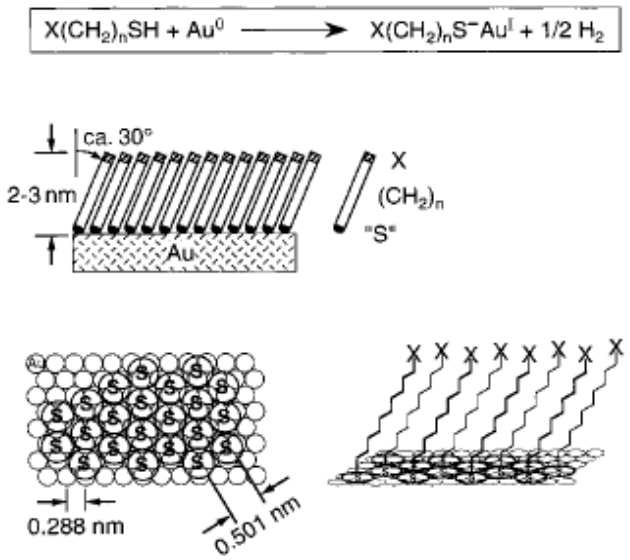

Figure 2.3 Formation of SAM on gold surface[47]

In an amperometric sensor, a carboxylic acid terminated SAM [$HS(CH_2)_nCOOH$ with n=15 or 11] is used to immobilize cytochrome c via carbodiimide activation.[49] A much bigger redox peak was found for covalently immobilized cytochrome c than electrostatically adsorbed cytochrome c. In addition, electrostatically driven adsorption is limited to low ionic strength solutions, because desorption occurs in high ionic strength solutions.[50,51] Covalent attachment allows for the characterization of cytochrome c over a wide range of solution conditions. Also, self-assembled monolayers of ω-mercapto carboxylic acids, $HS(CH_2)_nCOOH$ (n=2, 5, 10), on gold electrodes were applied to detect the neurotransmitter dopamine in the presence of ascorbic acid.[52] At neutral pH, the negatively charged SAM repels ascorbic acid, while positively charged dopamine

can be detected at sub-millimolar levels. An optimum value of n for the detection is n=5. This is attributed to a compromise between a well-organized system that requires long ω-mercapto carboxylic acids and a reasonable rate of electron transfer which is observed with short ω-mercapto carboxylic acids.

Redox enzymes linked to SAMs have been studied by Creager and Olsen.[53] A glucose sensor is prepared by cross-linking glucose (GOx) to a ω-hydroxy alkanethiol SAM through glutaric dialdehyde. Electrical communication between electrode and GOx is achieved via freely diffusing hydroxymethylferrocene. Normally, redox currents are diminished by a SAM, but the response of this redox mediator was less affected. Background currents due to interferences (uric acid, ascorbic acid and 4-acetamidophenol) were dramatically reduced relative to untreated electrodes. Willner et al.[54] achieved direct electron transfer by using a SAM-modified gold electrode. A roughened gold foil was first treated by cystamine to form a monolayer. This base monolayer was then reacted with pyrrploquinoline quinone (PQQ). After that, the resulting PQQ submonolayer was reacted with N-(2-aminoethyl)-FAD to yield a PQQ/FAD diad layer. Finally, apo-glucose oxidase was reconstituted on the PQQ/FAD monolayer-modified gold electrode. The process is shown in Figure 2.4. The enzyme layer in such an electrode provides efficient electrical contact with the electrode by PQQ redox relay and effectively stimulates the electrobiocatalyzed oxidation of glucose. The current increases linearly with increase of glucose concentration up to 80mM glucose. The current density attained is near the theoretical calculated value for a densely packed glucose oxidase monolayer.

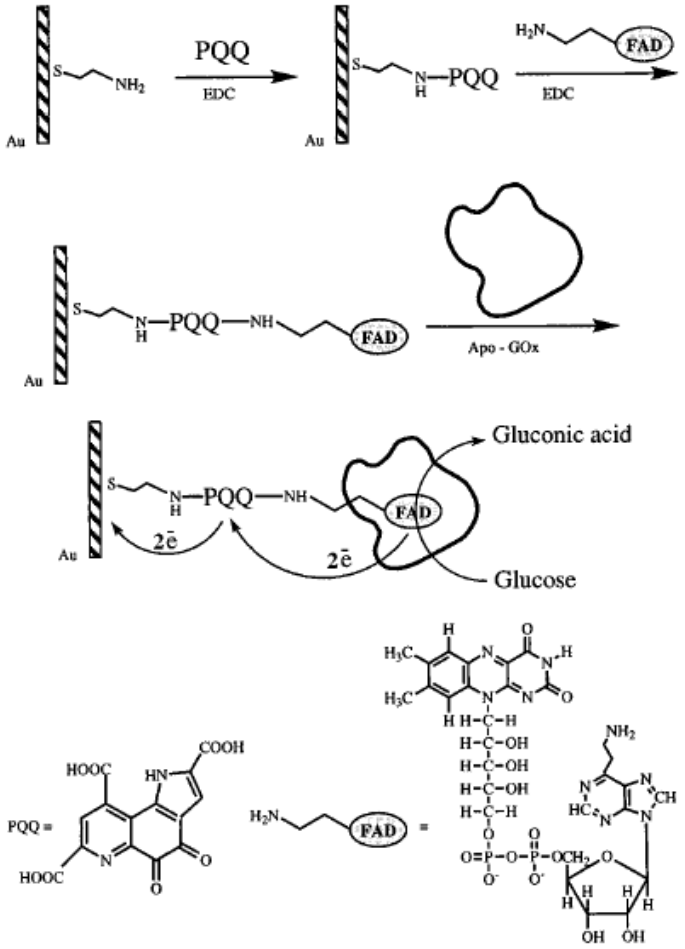

Figure 2.4 Reconstitution of glucose oxidase onto a PQQ/FAD monolayer Au-electrode and direct electron transfer between glucose and the modified electrode[54]

2.2.2 Electron-conducting Redox Hydrogels

Redox hydrogels constitute the only known electron-conducting phase in which the analyte (for example, glucose) and water-soluble ions dissolve and diffuse.[55] Redox polymers are comprised of two parts: the cross-linked backbone and tethered redox center. One typical structure is shown in Figure 2.5. The advantage of redox hydrogels is that the redox mediator is

covalently linked to the insoluble, but water-swollen, cross-linked polymer-network of the gel and the enzyme is also trapped in the gel so that there is no leachable component.[56-58] Another advantage is that multiple enzyme layers are connected to the electrodes and the attained current densities are usually about 10-fold higher or more than they are when enzyme monolayers are immobilized on the electrode surface. Mano et al.[58] studied the effect of the content of osmium to the current density of the enzyme electrode. They prepared three polymers with the [tethered complex (containing osmium)/pyridine/carboxyl-pentylpyridinium] ratio for polymer I being 10.7/85/4.3, for polymer II 12.8/85/2.2 and for polymer III 20/75/5. Compared with redox polymers I and III, the redox polymer II demonstrated the highest current density at 1.5 mA cm^{-2}. Besides, the oxidation of glucose on the enzyme electrode prepared with polymer II exhibited the lowest overpotential.

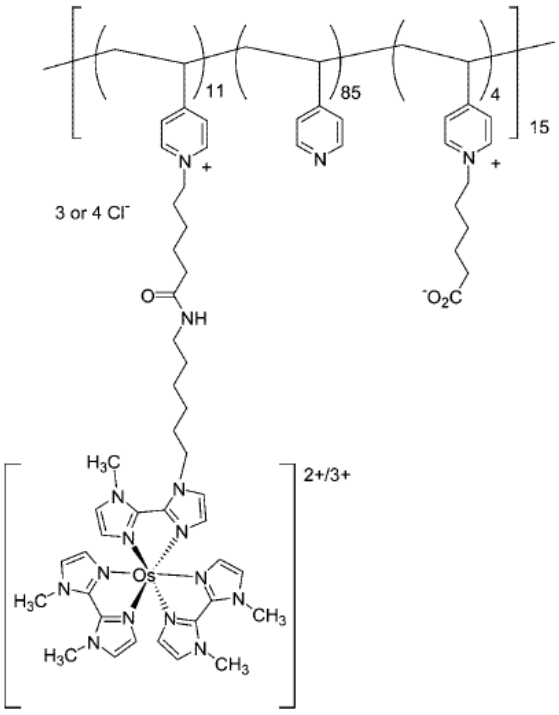

Figure 2.5 Structure of a redox polymer designed to electrically connect the reaction centers of glucose oxidase to electrodes[55]

Redox hydrogels conduct electrons by self-exchange of electrons or holes between rapidly reduced and rapidly oxidized redox functions tethered to backbones of cross-linked polymer networks. Although the networks, which are formed by cross-linking of water-soluble redox polymers, swell in water, they do not dissolve. The redox polymers conduct electrons, or holes, through self-exchange in water swollen hydrogels.[59] Because electron transfer by self-exchange requires collisions between reduced (electron-loaded) and oxidized (hole-loaded) redox centers,[59,60] electron transfer slows when an overwhelming majority of the redox centers are either oxidized or reduced. Another factor that affects the electron transfer rate is the spacers that connect the redox centers to the cross-linked networks. The long and flexible spacers increase the distance over which the tethered redox centers move about. In this way, more effective transferring collisions or faster electron transfer are achieved. The optimum spacers have lengths between 10 and 15 atoms.[57,61]

In a glucose biosensor, four electron transfer steps occur as shown in Figure 2.6. The electrons flow from glucose to the enzyme molecules (1), from the enzyme molecules to the redox polymer (2), through the redox polymer (3) and from the polymer to the anode (4). Thus, another important aspect in the redox hydrogel is the electron transfer between the enzyme and the tethered polymer. This is enabled by motion of the tethered segments of the cross-linked redox polymer network. After reacting with glucose, the redox center of glucose oxidase, FAD is reduced to $FADH_2$. It was then oxidized to FAD by collision with the tethered segments.

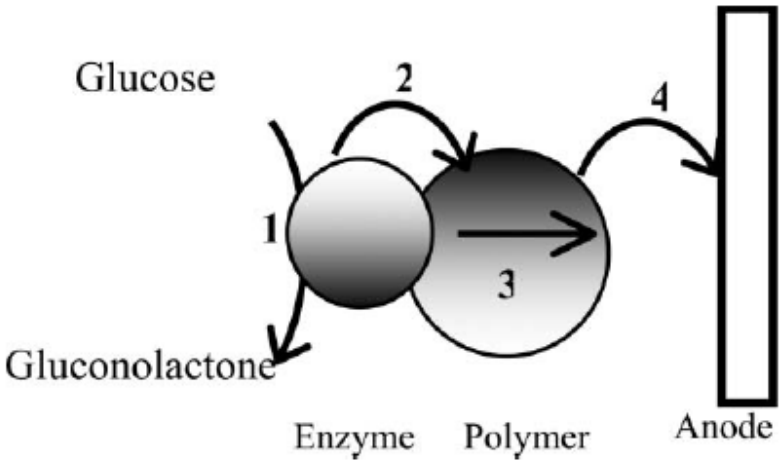

Figure 2.6 The electron transfer path in a glucose biosensor

Koide et al.[62] has studied the use of a ferrocene-containing polymer. The structure of this polymer is shown in Figure 2.7. Polyallylamine was cross-linked with glutaraldehyde and modified successively with ferrocenecarboxylic acid. GOx and the redox hydrogel were immobilized on the glassy carbon electrodes by using glutaraldehyde. They found that swelling of the redox polymer caused a decrease of the redox current because this increased the distance between the redox sites of the polymer and slowed down electron transfer rate among neighboring redox sites. However, by adding bovine serum albumin (BSA) into this polymer, excessive swelling could be prevented and the redox polymer maintained its original redox current even after 5 h of soaking. The linear range between current and glucose concentration extends as far as 7mM.

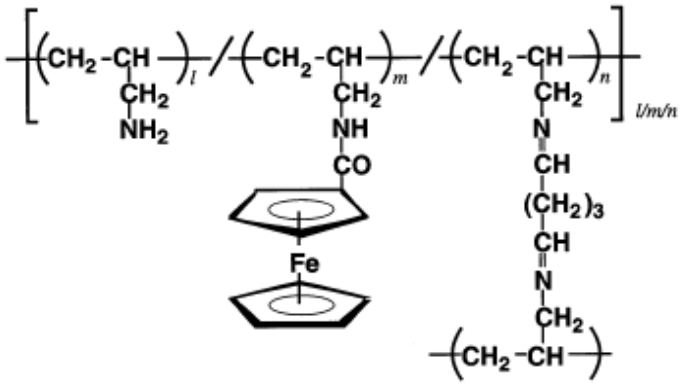

Figure 2.7 Structure of ferrocene-containing cross-linked polyallylamine[62]

2.2.3 Carbon Nanotubes and Other Nanomaterials

Carbon nanotubes (CNT) discovered by Iijima in 1991[63] have gained considerable attention in recent years because of their remarkable electronic and mechanical properties, which have made them extremely attractive for a wide range of sensing applications from structural materials[64] to nanoelectronic components.[65] One advantage of the application of CNT in biosensing is direct electron transfer. Cai et al.[66] studied the direct electron transfer of glucose oxidase promoted by multi-walled carbon nanotubes. CNT was first dispersed in a solution of surfactant, cetyltrimethylammonium bromide (CTAB). Then, this CNT suspension was mixed with GOx, thus caused the physical adsorption of GOx molecules onto the surface of CNT during mixing. An aliquot of this mixture was cast onto glassy carbon electrode surface and dried. Finally, Nafion was used as a binder to hold the GOx-CNT on the electrode surface stably. Cyclic voltammograms of this Nafion-GOx-CNT/GC electrode in 0.1M PBS (pH 6.9) at a scan rate of 40mV/s showed a pair of well-defined and nearly symmetric redox peaks (Figure 2.8). From the

dependence of ΔE_p on the scan rates, the apparent heterogeneous electron transfer rate constant, k_s, was calculated to be $1.53 \pm 0.45 s^{-1}$.

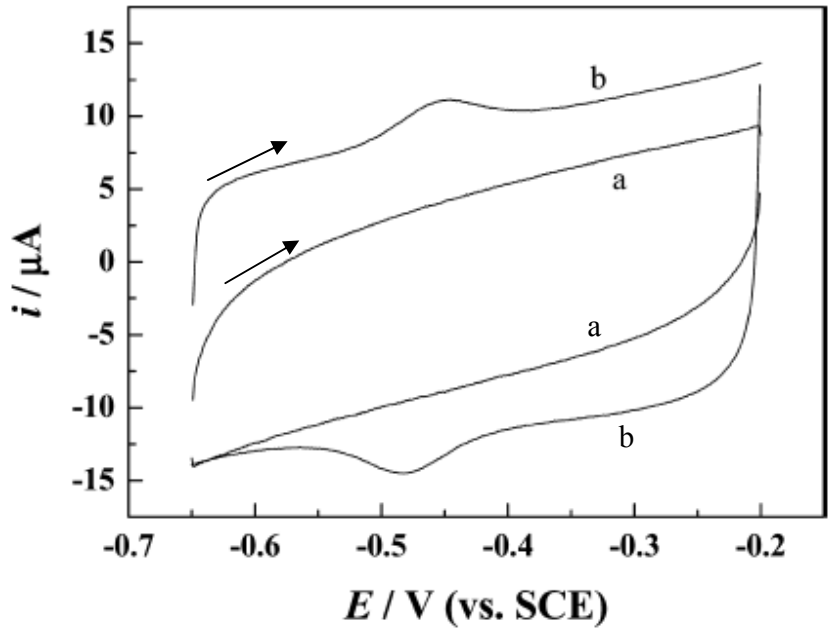

Figure 2.8 Cyclic voltammograms of the the Nafion-CNT/GC (a) and Nafion-GOx-CNT/GC (b) electrode in 0.1M PBS (pH 6.9) at a scan rate of 40mV/s. The arrows denote the scan direction.[66]

Gooding et al.[67] presented a strategy for studying the electron transfer properties of redox enzymes such as microperoxidase 11 attached to the end of aligned single-walled carbon nanotubes (SWCNT). Rather than coating the electrode surface by a random tangle of nanotubes,[68-73] SWNTs were aligned on the electrode surface. A polycrystalline gold electrode was first activated by cystamine to form a cystamine self-assembled monolayer (SAM). This electrode was further treated by shortened SWCNTs in DMF containing dicyclohexylcarbodiimide to convert the carboxyl group located at the end of the shortened SWCNTs into active carbodiimide esters. The SWCNTs were aligned normal to the electrode

surface. Finally, microperoxidase was attached to the free ends of the tubes by incubation in a microperoxidase solution at 4°C overnight. This process is shown in Figure 2.9. The SWCNTs aligned on the electrode surface were able to wire electron transfer between the protein and gold electrode.

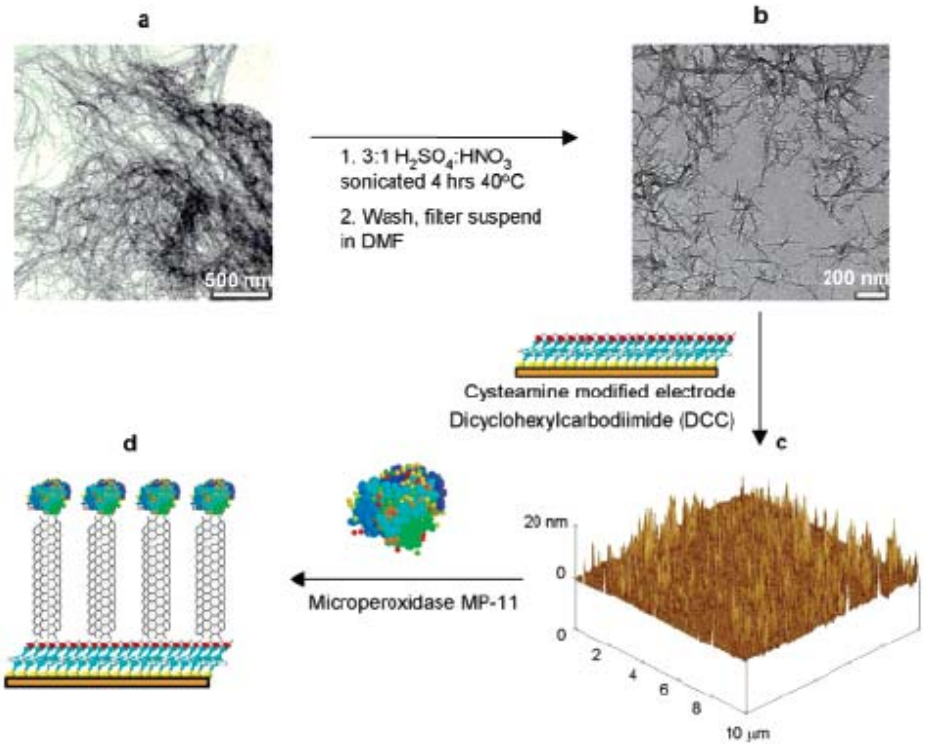

Figure 2.9 Scheme of the different steps involved in a fabrication of aligned shortened SWCNT arrays for direct electron transfer of microperoxidase MP-11[67]

A similar strategy was used by Patolsky et al.[74] for constructing a glucose biosensor. A 2-thioethanol/cystamine mixed monolayer (3:1 ratio) was assembled on a gold electrode and the SWCNTs were attached to the surface in the presence of the coupling reagent 1-ethyl-3-(3-dimethylaminopropyl) carbodiimide hydrochloride (EDC) as depicted in Figure 2.10. The amino

derivative of the FAD cofactor was then coupled to the carboxy groups at the free edges of the standing SWCNTs. Finally, apo-GOx was reconstituted on the FAD units linked to the ends of the standing SWCNTs. The result demonstrated that the SWCNTs act as nanoconnectors that electrically connect the active site of the enzyme and the electrode. The electron transfer rate is controlled by the length of the SWCNTs. The longer the nanotube is, the slower is the transfer rate. This enzyme electrode also showed good capability for glucose sensing and has a detection range as high as 160mM glucose.

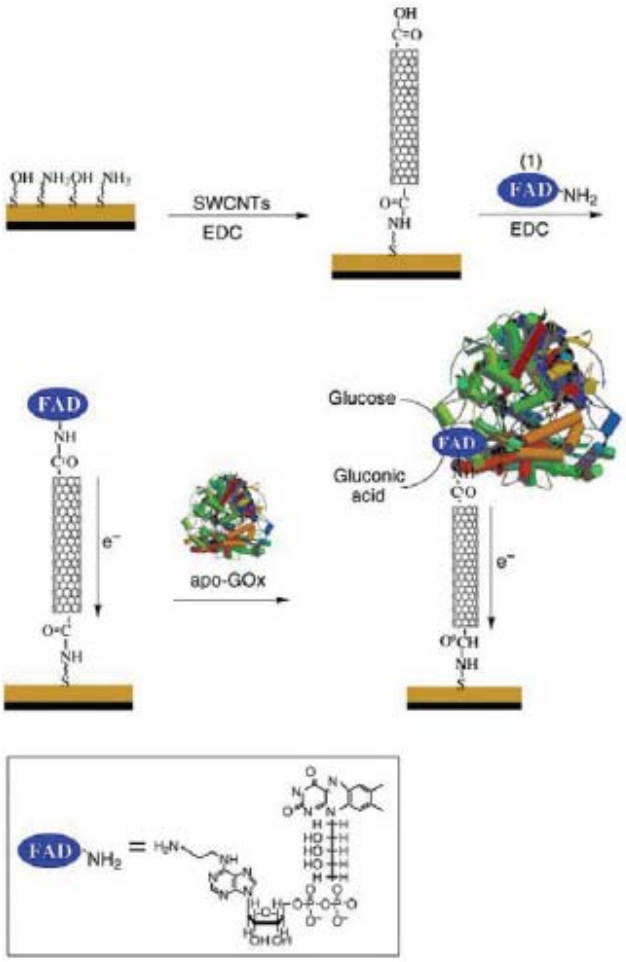

Figure 2.10 Fabrication process for electrically wiring glucose oxidase to a nanotube electrode[74]

Yemini et al.[75,76] explored the use of peptide nanotubes (PNT) in biosensors. Dipeptide phenylalanine-phenylalanine (FF) was found to form nanotube structures. The diphenylalanine-based peptide nanotubes have many advantages as they are biocompatible, can be easily modified with biological and chemical elements,[77-79] and show a notable similarity to carbon nanotubes in their morphology and aspect ratio. The PNT was first used to modify screen printed electrodes. Ferri/ferrocyanide was used as a probe to test the electrochemical properties of the PNT-modified electrodes. Cyclic voltammograms showed that after modification, the redox current for $K_4[Fe(CN)_6]/K_3[Fe(CN)_6]$ increased about 2-fold. The difference between E_{pa} and E_{pc} decreased from 0.14V for unmodified screen printed electrodes to 0.07V for PNT-modified electrodes. These results indicate that the presence of peptide nanotubes significantly improved the electrochemical fingerprint of the electrode. This peptide nanotube-modified electrode was then further tested for the application of H_2O_2 sensing. Again, a much higher current response was obtained with the PNT-modified electrode than the bare screen-printed electrode.

The peptide nanotubes have also been modified by a thiol group and used to modify a gold electrode.[76] This modified gold electrode showed a good amperometric response to detect hydrogen peroxide and NADH. The high electrocatalytic activity of PNT modified electrode is likely due to the direct electron transfer between the spatially aligned aromatic systems that contribute to the electronic conductivity of the assemblies. Furthermore, GOx was immobilized onto the PNT-modified gold electrode and showed a linear amperometric response upon successive addition of 0.2mM glucose.

2.3 Peptide Self-assembly

Self-assembly is defined as the process whereby individual components spontaneously organized into an ordered structure without any artificial intervention.[80] The mechanism behind the self-assembly phenomena is weak, non-covalent interactions between individual elements. Self-assembly peptides have been extensively studied during the last decade. There are 20 natural amino acids that are the building blocks for various peptides. The easy preparation and purification of short peptides makes them very useful for peptide design and studying of the relationship between their molecular structure and physiochemical properties. Several types of self-assembly peptides are reviewed in the following sub-sections.

2.3.1 Amphiphilic and Surfactant Peptides

The traditional surfactant contains a hydrophobic region and a separate hydrophilic region that can self-assemble into distinct structures such as micelles, vesicles and tubules. The driving force is mostly that the hydrophobic part of the surfactant tends to avoid the water phase and approaches the hydrophobic part of the other surfactant molecules. The same idea can be used for the design of amphiphilic peptides. Zhang's group from MIT has done a lot of work on the amphiphilic peptides.[81-85] These peptides share a common motif: the polar region of each molecule has one or two charged amino acids and the non-polar region is made from four or more consecutive hydrophobic amino acids.

One example[84] is V_6D with the sequence of VVVVVVD (V denotes valine and D denotes aspartic acid). It has a hydrophilic head of negatively charged aspartic acid (D) containing another negative charge from the C terminus. The hydrophobic tail contains six valines (V) and the N terminus is acetylated, making it uncharged. From dynamic light scattering (DLS) test, this

peptide self-assembles into 30-50nm structures when dissolved in water. In order to determine the real structure of the peptide formed in aqueous solution, a transmission electron microscopy (TEM) study of the flash-frozen samples was conducted. The result is shown in Figure 2.11. Nanotube structures with approximately 30-50nm diameters that are several microns long are clearly seen from the TEM images. Nanovesicles were also observed, suggesting that dynamic behavior of the supramolecular assemblies may be tunable by changing the environment and the sequence of the monomer.

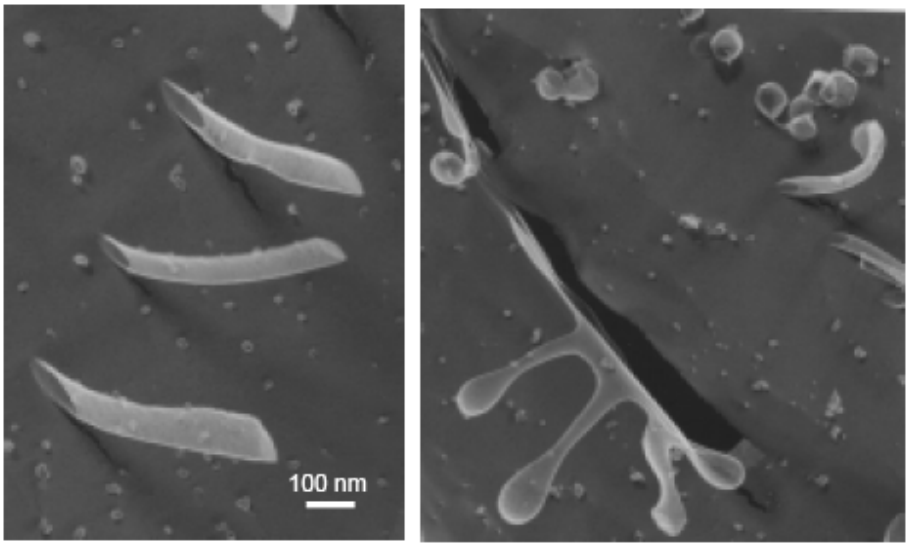

Figure 2.11 The TEM images of V6D. The sample was flash-frozen in liquid propane (-180°C) and surface-coated with a thin layer of platinum and carbon, yielding a replica to preserve the structures formed in solution.[84]

A proposed pathway for the formation of this supramolecular structure of nanotubes is shown in Figure 2.12. The peptide monomers form small segments of the bilayer ring, with hydrophobic tails packing together to avoid water and hydrophilic heads exposed to water on the

inner and outer portion of the tube. Through continuous dynamic energy minimization, they grow into single subunit rings and multirings, in which aspartic acid hydrophilic groups remain exposed to the continuous aqueous medium. The tubular arrays may subsequently stack through noncovalent interactions to form longer nanotubes.

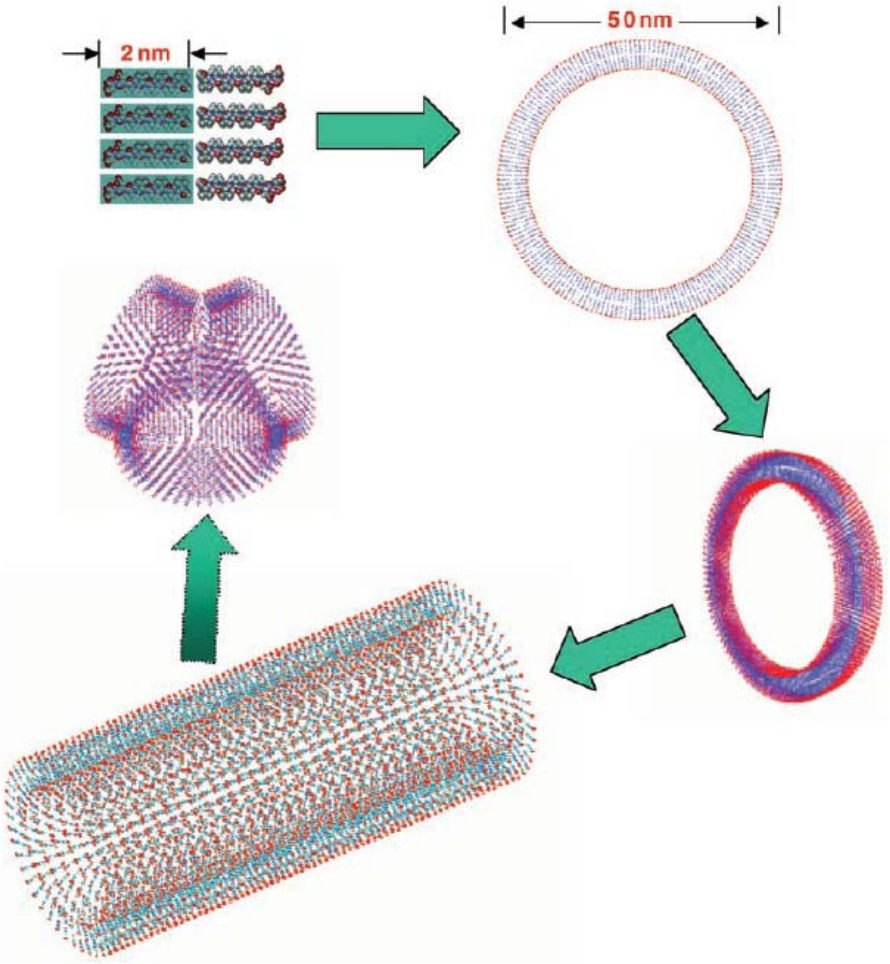

Figure 2.12 Potential pathway of V6D peptide nanotube formation. Each peptide monomer is 2nm, and the diameter of the modeled bilayer nanotube is 50nm. Red, hydrophilic head; blue, hydrophobic tail. Each peptide may interact with one another to form closed rings, which in turn stack on top of one another, ultimately yielding a nanotube. Three nanotubes are connected to each other through a three way junction.[84]

Table 2.1 List of peptide amphiphiles[86]

Molecule	N terminus	Peptide (N to C)	Charge pH 7
1	H	CCCCGGGS$^{(PO_4)}$RGD	−2
2	$C_6H_{11}O$	CCCCGGGS$^{(PO_4)}$RGD	−3
3	$C_{10}H_{19}O$	CCCCGGGS$^{(PO_4)}$RGD	−3
4	$C_{16}H_{31}O$	CCCCGGGS$^{(PO_4)}$RGD	−3
5	$C_{22}H_{43}O$	CCCCGGGS$^{(PO_4)}$RGD	−3
6	$C_{10}H_{19}O$	AAAAGGGS$^{(PO_4)}$RGD	−3
7	$C_{16}H_{31}O$	AAAAGGGS$^{(PO_4)}$RGD	−3
8	$C_{16}H_{31}O$	CCCCGGGS$^{(PO_4)}$	−3
9	$C_{16}H_{31}O$	CCCCGGGS$^{(PO_4)}$KGE	−3
10	$C_{16}H_{31}O$	CCCCGGGS$^{(PO_4)}$RGDS	−3
11	$C_{16}H_{31}O$	CCCCGGGSRGD	−1
12	$C_{16}H_{31}O$	CCCCGGGEIKVAV	−1

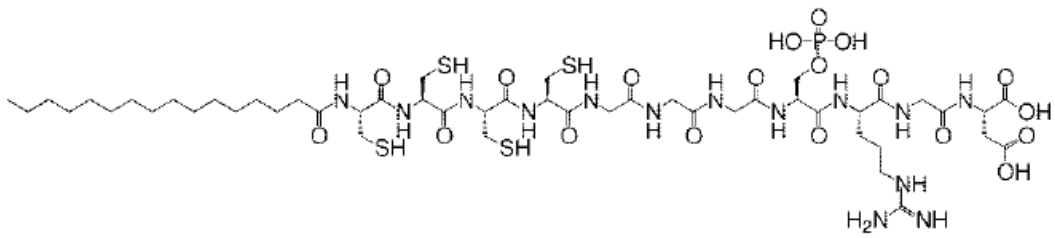

Figure 2.13 Structure of PA4[86]

Hartgerink et al.[86] designed a series of peptide-amphiphiles (PAs) and studied their self-assembly properties in aqueous solution. The PAs are listed in Table 2.1. The structure of one of these PAs, PA4, is shown in Figure 2.13. They found that the self-assembly of PAs is sensitive to pH. When the pH of the solution is neutral, the PAs are negatively charged so that the peptide molecules repel each other and self-assembly of PAs is suppressed. Upon acidification, the negative charges are eliminated and the hydrophobic tails begin to aggregate. However, this

aggregation of the hydrophobic tails is also dictated by the length of the tails. PA1 does not self-assemble because the tails are not long enough so that the hydrophobic interaction is not strong enough to induce self-assembly. PAs 3-5 have sufficiently long hydrophobic tails to make the cylindrical packing the most favorable. However, if PAs 3-5 are oxidized and form intramolecular disulfide bonds, the formation of nanofibers is not observed, indicating that conformational changes induced by these disulfide bonds suppress self-assembly. The assembly of PA4 can be triggered by pH. At pH4, it can form nanofiber networks with fibers that are ~7nm in diameter and several microns in length. These nanofibers can direct the growth of hydroxyapatite crystals, mimicking the function of collagen fibers in bone tissue. A three-amino acid moiety of arginine-glycine-aspartic acid (RGD) is attached to the carboxy-terminal of the peptide since this sequence has been found to be important in cell adhesion. Its incorporation into the system may promote cellular adhesion and overall biocompatibility.[87]

Cyclic peptides consist of six or eight amino acids with alternating D- and L- enantiomers. By means of elegant structural design, they can stack into nanotubes (Figure 2.14).[88,89] The stack of the peptides is dependent on pH based on their amino acid sequences. The stacking can be controlled by selective protonation of the amino acid residues on each cyclic peptide disk at different pH values.[89] This peptide system demonstrates some important applications for nanobiotechnology. First, assembled nanotubes could be used as an antibacterial agent since they act preferentially on bacterial membranes to increase their permeability and collapse transmembrane ion potentials. Furthermore, these actions lead to cell death. Second, the physical properties of the nanotube interiors can be modified by introducing heterocyclic alterations that allow for the passive transportation of small molecules.

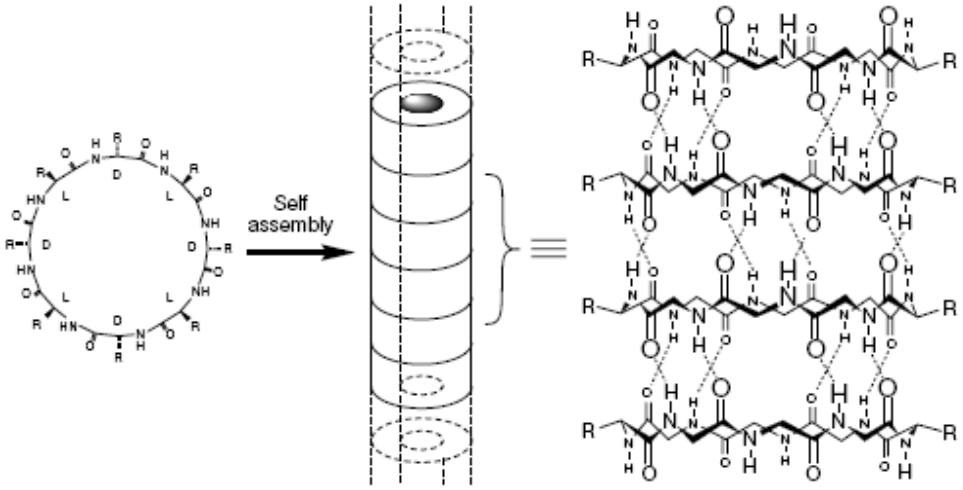

Figure 2.14 Self-assembly of eight-residue cyclic D,L-α-peptides into nanotubes. The self-assembly of the eight residue cyclic D,L-α-peptides with a flat and ring-shaped conformation is directed by backbone-backbone hydrogen bonding to give β-sheet-like tubular supramolecular structures. These nanotubes are open-ended and hollow.[88]

2.3.2 Ionic-complementary Peptides

Along with the development of peptide amphiphiles and surfactant-like peptides, ionic-complementary peptides have emerged as promising materials for many biomedical applications. Ionic-complementary peptides are characterized by an alternating arrangement of negatively and positively charged residues. There are certain patterns of charge distribution that the peptides should follow so that the sequence can have ionic-complementary property. The most simple and widely used patterns are type I (- +), type II (- - + +) and type IV (- - - - + + + +). The major force

that promotes peptide self-assembly in this case is electrostatic interactions. The various ionic-complementary peptides that have been studied are listed in Table 2.2.

Table 2.2 The list of ionic-complementary peptides[90-92]

Name	Sequence	Charge Distribution	Type	Structure
P_{11}-I	n-QQRQQQQQEQQ-c	+−	I	α/β
P_{11}-II	n-QQRFQWQFEQQ-c	+−	I	α/β
P_6-1	n-KTVIIE-c	+−	I	β/r.c.
P_6-6	n-KTVLIE-c	+−	I	β/r.c.
P_6-7	n-KTVIVE-c	+−	I	β/r.c.
P_6-8	n-KTVIYE-c	+−	I	r.c.
$A\beta_{16-22}$	n-KLVFFAE-c	+−	I	α/β/r.c.
KADA8-I	n-KADAKADA-c	+−+−	I	r.c.
KFE8-I^T	n-KFEFKFEF-c	+−+−	I	β
KFE8-I	n-FKFEFKFE-c	+−+−	I	β
RADA8-I	n-RADARADA-c	+−+−	I	r.c.
RAEA8-I	n-RAEARAEA-c	+−+−	I	r.c.
EFK8-I	n-FEFKFEFK-c	−+−+	I	β
EAKA8-I	n-AEAKAEAK-c	−+−+	I	r.c.
KFE12-I	n-FKFEFKFEFKFE-c	+−+−+−	I	β
KIE12-I	n-IKIEIKIEIKIE-c	+−+−+−	I	β
KVE12-I	n-VKVEVKVEVKVE-c	+−+−+−	I	β
KLD12-I	n-KLDLKLDLKLDL-c	+−+−+−	I	β
KLE12-I	n-KLELKLELKLEL-c	+−+−+−	I	β
EFK12-I	n-FEFKFEFKFEFK-c	−+−+−+	I	β
RADA16-I	n-RADARADARADARADA-c	+−+−+−+−	I	β
RGDA16-I	n-RADARGDARADARGDA-c	+−+−+−+−	I	r.c.
RAEA16-I	n-RAEARAEARAEARAEA-c	+−+−+−+−	I	β
KADA16-I	n-KADAKADAKADAKADA-c	+−+−+−+−	I	β
KFE16-I	n-FKFEFKFEFKFEFKFE-c	+−+−+−+−	I	β

EAKA16-I	n-AEAKAEAKAEAKAEAK-c	−+−−−+−+	I	β
RAD8-II	n-RARADADA-c	++−−	II	r.c.
EAH8-II	n-AEAEAHAH-c	−−++	II	r.c.
ELK8-II	n-LELELKLK-c	−−++	II	β
EAK8-II	n-AEAEAKAK-c	−−++	II	r.c.
EAK12-a	n-AKAKAEAEAKAK-c	++−−++	II	r.c.
RAD16-II	n-RARADADARARADADA-c	++−−++−−	II	β
EAH16-II	n-AEAEAHAHAEAEAHAH-c	−−++−−++	II	β
EFK16-II	n-FEFEFKFKFEFEFKFK-c	−−++−−++	II	β
ELK16-II	n-LELELKLKLELELKLK-c	−−++−−++	II	β
EAK16-II	n-AEAEAKAKAEAEAKAK-c	−−++−−++	II	β
KAE16-IV	n-KAKAKAKAEAEAEAEA-c	+++−−−−	IV	β
RAD16-IV	n-RARARARADADADADA-c	+++−−−−	IV	β
EAK16-IV	n-AEAEAEAEAKAKAKAK-c	−−−−++++	IV	β
DAR16-IV	n-ADADADADARARARAR-c	−−−−++++	IV	α/β
DAR16-IV^{T}	n-DADADADARARARARA-c	−−−−++++	IV	α/β
DAR32-IV	n-(ADADADADARARARAR)$_2$-c	−−−−++++	IV	α/β
EAK12-b	n-AKASAEAEAKAK-c	+−−++	N/A	r.c.
EAK12-c	n-AKAEAEAEAKAK-c	+−−−++	N/A	r.c.
EAK12-d	n-AEAEAEAEAKAK-c	−−−−++	IV/II	α/β

Note: β: β-sheet; α: α-helix; r.c.: random coil; N/A: not applicable.

Ionic-complementary peptides have some unique characteristics. First of all, their charge distribution can be altered by the design of the sequence. For example, using the same amino acids (E, A and K) as the building blocks, three typical peptides can be designed, EAK16-I, EAK16-II and EAK16-IV (see Table 2.2). The difference in the charge distribution types can influence the peptide secondary structure and therefore its self-assembly.

A second feature, particular to the ionic-complementary peptides first studied by Zhang et al, is the specific chain lengths required to exhibit ionic complementary. The length of these peptides varies from eight to thirty-two amino acids in sequence due to alternating hydrophobic and

hydrophilic residues in the peptide sequence. The minimum number of amino acids required to build type I peptides is four, while type II and type IV require eight and sixteen amino acids, respectively.

A third feature is that the ionic-complementary peptide family can be easily expanded with the same charge distribution by using different amino acids. For example, starting from EAK16-II, many other similar peptides can be derived. Glutamic acid (E) can be replaced by aspartic acid (D), which is also negatively charged at neutral pH; on the other hand, lysine (K) can be replaced by arginine (R), which is positively charged at neutral pH. The hydrophobic residue of EAK16-II, alanine (A), can also be replaced by hydrophobic amino acids such as phenylalanine (F) and leucine (L). Such simple replacement maintains the intrinsic properties of ionic-complementarity and self-assembly.

Ionic-complementary peptides are promising molecules for material engineering because they can form stable nano/microstructures. In order to regulate its nano/microstructure, the understanding and precise control of peptide self-assembly is always a big challenge for material scientists. Using EAK16s as model peptides, our group has conducted a large amount of research toward controlling its self-assembly. The details will be discussed in the following.

Sequence effect on self-assembly

Peptide sequence serves as an internal factor that tunes their self-assembly. The type, number and arrangement of amino acids in the sequence are extremely important in determining the secondary structures and self-assembly of the peptides. Each amino acid component has its own propensity to form a specific secondary structure. In addition, the periodicity of hydrophobic and hydrophilic amino acid residues can affect the secondary structure of a peptide.

Hong et al.[93] reported the effect of amino acid sequence on the nanostructure of self-assembling peptides. They investigated the nanostructure formed by EAK16-II and EAK16-IV at different pH values, using atomic force microscopy (AFM). EAK16-II and EAK16-IV have the same amino acid components but different charge distributions, resulting in different polarities. The AFM images showed that EAK16-II formed well-defined fiber networks, whereas EAK16-II formed globular nanostructures at neutral pH (Figure 2.15). Further investigation showed that EAK16-II formed fibril assemblies when prepared at pH values between 4 and 11, where EAK16-IV formed globular assemblies only near neutral pH (pH 6.5-7.5). When prepared above pH 7.5 or below pH 6.5, EAK16-IV formed fibril assemblies that were indistinguishable from the fibrils formed by EAK16-II. Surface tension studies suggested that there is a significant correlation between peptide nanostructure and surface activity. The globular EAK16-IV assemblies have lower surface tension, indicating a higher hydrophobicity than the fibril EAK16-II assemblies. This could be due to the bending of EAK16-IV via strong intramolecular electrostatic attraction to form β-turns, exposing hydrophobic residues to the solution and lowering the surface tension. On the other hand, EAK16-II prefers a stretched β-strand, resulting in linear fibrils.

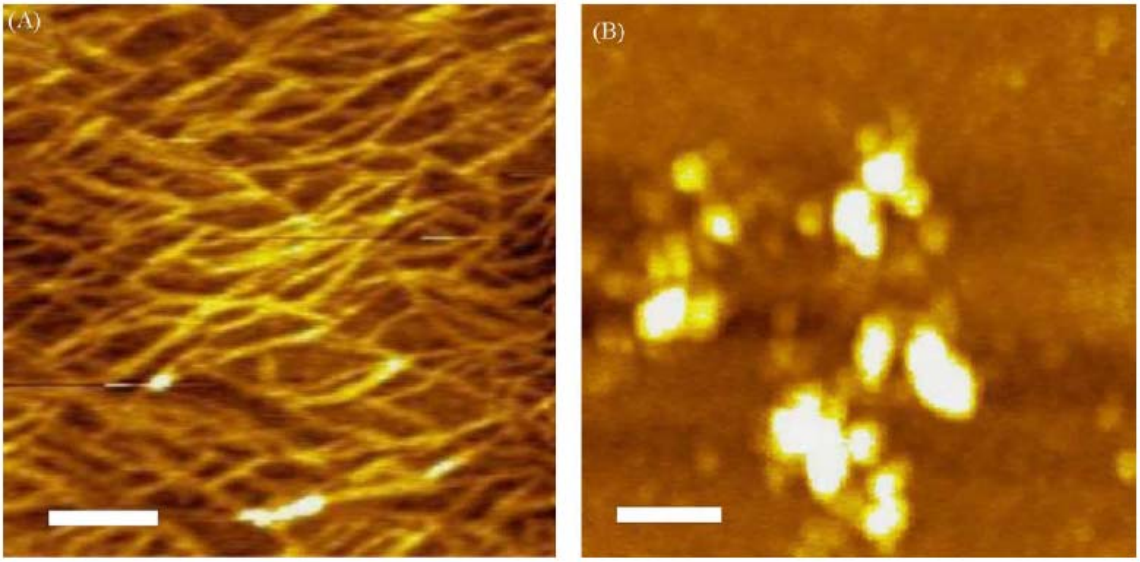

Figure 2.15 AFM images of EAK16-II (A) and EAK16- IV (B). The scale bars are 200nm.[93]

Concentration effect on self-assembly

Another factor that affects self-assembly is peptide concentration. Since the peptide has a structure containing both hydrophobic and hydrophilic residues, the concentration dependence of peptide self-assembly is expected to be similar to that of surfactants. The micelle formation of surfactants has a critical micelle concentration (CMC). Similarly, one may anticipate that the peptides would be dispersed in a solution below a critical aggregation concentration (CAC) and begin to aggregate at or above this concentration. A CAC has been reported for many proteins and amphiphilic pepties.[94-97] Alzheimer's Aβ peptides have a CAC of 25μM at neutral pH[96,97] and 100μM in 0.1M HCl.[97]

Fung et al. found EAK16-II has a CAC value of ca. 60μM.[98] The experiment was conducted by measuring the surface tension of peptide solution at different concentrations. The equilibrium surface tension was plotted against the peptide concentration and a transition state found to occur

at around 60μM, corresponding to the CAC. AFM studies of the nanostructure of EAK16-II revealed that isolated filaments and globules form below CAC while fibril network forms above CAC. In addition, the fibril size and network density are also dependent on the concentration. Another peptide EAK16-I was also investigated and the CAC was found to be 180μM.[99]

pH effect on self-assembly

pH and salt concentrations are two significant factors in determining protein and peptide structures in biological systems. Since the peptides are composed of different amino acids, the change in solution pH can affect the ionic state of some amino acids as well as the net charges of peptides. This further influences the self-assembly behaviour because amino acid charges play an important role in determining the aggregation of the peptides. For example, polylysine undergoes structural changes from an α-helix to a β-sheet above pH 10 when the lysine residues became protonated[100,101]. This conformational change is reversible when the pH is lowered. Similarly, the β-amyloid peptide also goes through a structural change when the pH changes. It forms β-sheet structures at pH 5.4 and helical structures at pH 3 or 8.3[101]. These results suggest that the charge state of amino acid is critical to the secondary structure of peptides.

The nanostructure of ionic-complementary peptides was studied by Hong et al.[93] using AFM. Interestingly, they found that the dependence of nanostructure on pH changes is different according to the peptide charge distribution. EAK16-IV formed globular structure at pH between 6.5 and 7.5, while nanofiber structures appear at pH below 6.5 or above 7.5. In contrast, EAK16-II formed fibril nanostructures throughout the pH range from 4 to 11. These finding suggest that the charge distribution in sequence plays an important role in determining the self-assembled peptide nanostructures. For a type IV charge distribution, strong intramolecular electrostatic

attractions occur at neutral pH and result in globular nanostructures. At extreme pHs such as pH 4 and 11, either glutamic acid or lysine residues are neutralized. Therefore, intramolecular electrostatic interaction is weakened and insufficient to cause the peptide to form globular assembly. Thus, nanofiber formation will be predominant.

Salt effect on self-assembly

The presence of salt affects the conformation and properties of many biological molecules, including their stability, solubility and biological activity[102]. The self-assembly of biomolecules is affected by salt concentration, valency of the salt, or even replacement of one type of salt with another of the same valency[103]. Chen et al. reported the effect of salts on peptide self-assembly[99]. The CAC of EAK16-I increased in the presence of salts. Surface tension and AFM measurements showed that EAK16-I has a CAC of about 0.3mg/ml in water. In the presence of 20mM NaCl, the critical aggregation concentration of the peptide increased to 0.8mg/ml. The reason for this phenomenon is still not clear. De al Paz and colleagues found NaCl has significant effect on amyloid fibril formation[104]. By incubating the peptide in salt solution, they found that over the NaCl concentration range of 0-0.1M, the rate of fibril formation increased with ionic strength. At higher concentrations (>0.1M), only short filaments and amorphous aggregates could be observed.

Surface effect on self-assembly

Molecular assembly at a surface plays an important role in many nanotechnology and biological applications. The effect of surface on the self-assembly of peptides and proteins has been explored in a variety of nanosystems. For example, the negatively charged virus M13 can

spontaneously form ordered monolayer structures on the surface of a positively charged, multilayered LPEI/PAA polymer film[105]. In another example, a hydrophobic graphite surface was reported to direct molecules, such as peptides[106-108] and polymers[109] to organize into various patterns. Yang et al.[110] reported the self-assembly of ionic-complementary peptide EAK16-II on a mica surface. *In-situ* AFM was used as a main tool to observe the self-assembly of EAK16-II on this surface. Through real-time observation of EAK16-II nanofiber growth on mica, it was found that the nanofiber growth follows a nucleation and growth mechanism. The nanofiber "seeds" or fiber clusters formed in stock solution first adsorb on mica surface and serve as nuclei; this is followed by fiber elongation at the active ends of these nuclei. In addition, dynamic light scattering experiments showed that nanofibers no longer growing in solution can start to grow once they adsorb onto the surface and indicate that the nanofiber growth is a surface-assisted phenomenon. A proposed model is shown in Figure 2.16. Further research found that the growth rate of nanofiber can be regulated by adjusting the solution pH. The growth rate in different solutions follows the order: pure water > 1mM HCl > 1mM NaOH >10mM HCl ≈ 10mM NaOH ≈ 0.

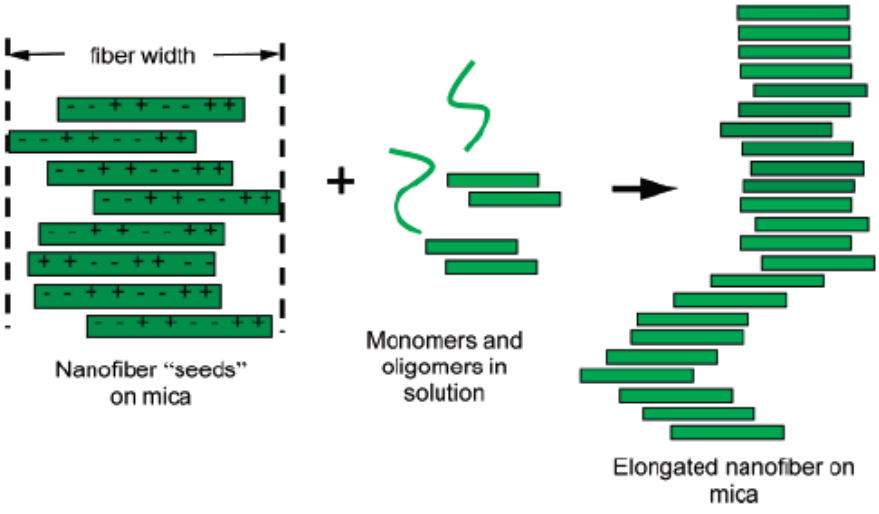

Figure 2.16 Proposed model of EAK16-II nanofiber growth on mica[110]

Chapter 3 Improved Enzyme Immobilization on an Ionic-complementary Peptide Modified Electrode for Biomolecular Sensing

3.1 Introduction

Biosensors are devices that are comprised of a biologically sensitive element (bio-recognition agent) and a transducer so as to transform chemical information (e.g., concentration of specific compounds) into an analytically useful signal.[1,5] Among various biosensors, glucose biosensors have emerged as one of the most intensely studied because glucose detection is essential for both blood sugar monitoring of diabetes patients[111] and quality control in food processing industries[112]. Since Clark and Lyons first proposed the initial concept for glucose enzyme electrodes[113] in 1962, tremendous efforts have been directed towards their development with upgraded sensitivity and stability[54,55,66,114,115].

One essential step in the fabrication of an amperometric glucose biosensor is the immobilization of an enzyme, which is usually glucose oxidase (GOx)[116], onto the surface of electrodes. For this purpose, various materials have been used, such as polymers[117], sol-gels[118] and self-assembled monolayers (SAMs)[119]. With recent developments in nanotechnology and bio-materials, researchers have begun to use peptide-modified electrodes for enzyme immobilization. Yemini el al. [75] reported a novel electrochemical biosensing platform based on self-assembled diphenylalanine (FF) peptide nanotubes. They demonstrated that the $Fe(CN)_6^{4-}$ /$Fe(CN)_6^{3-}$ redox couple was more reversible and exhibited higher anodic/cathodic peak currents

on peptide nanotube-modified electrodes. Their research[76] further showed that peptide nanotube-modified gold electrodes can be used to immobilize GOx for glucose detection. However, the peptide nanotube based biosensor had a low sensitivity compared to other glucose biosensors. In addition, the storage stability of this kind of biosensor remains a serious problem. A collagen-like peptide modified gold electrode has also been studied for enzyme immobilization in biosensors[120], whereby horseradish peroxidase (HRP) was covalently immobilized for H_2O_2 detection. The peptide layer on the electrode surface not only provided functional groups for enzyme immobilization, but also provided a biocompatible environment. However, this sensor also had the problem of low sensitivity.

In previous work done by our research group, Yang et al.[121] demonstrated that ionic-complementary, self-assembling peptides can be applied to the immobilization of GOx and the fabrication of a glucose biosensor. Similar to the collagen-like peptide layer, this unique ionic-complementary peptide assembly also provides both functional groups and a biocompatible environment. To further develop applications for ionic-complementary peptides in biosensing, we present in this work a method for improving enzyme immobilization and thus achieving increased sensitivity of the sensor.

A typical ionic-complementary peptide EFK16-II was used in this study. Its molecular structure is shown in Figure 3.1. Two different methods for the immobilization of the enzyme GOx on the peptide modified HOPG electrode were compared. The first method is that described by Yang et al[121]. The peptide-modified HOPG electrode was first activated by a carbodiimide agent. Then enzyme was then immobilized onto this activated surface. However, cross-linking of the peptide was suspected to occur during the activation process, so that fewer active enzyme molecules were likely to be immobilized. In the second immobilization method, the peptide-

modified HOPG electrode was not activated by carbodiimide. Instead, the carbodiimide was initially mixed with the enzyme in a buffer solution and this solution was injected onto the peptide modified HOPG surface for enzyme immobilization. This small change in the process resulted in a significant difference in terms of active enzyme immobilization and sensor performance.

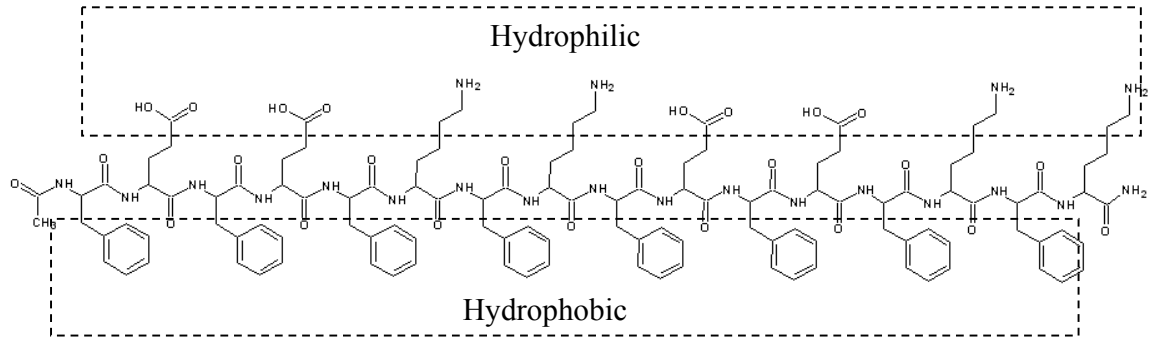

Figure 3.1 Molecular structure of EFK16-II. The amino acid sequence is FEFEFKFKFEFEFKFK. The lower side is hydrophobic due to the phenylalanine (F) residues; the upper side is hydrophilic due to the glutamic acid (E) and lysine (K) residues.

3.2 Materials and Methods

3.2.1 Materials

The ionic-complementary peptide FEFEFKFKFEFEFKFK (EFK16-II) was purchased from CanPeptide Inc. (Quebec, Canada) and used without further purification. In the peptide sequence,

F, E and K denote phenylalanine glutamic acid and lysine, respectively. The N-terminus and C-terminus of the peptide were protected by acetyl and amino groups, respectively.

Highly ordered pyrolytic graphite (HOPG, 1cm × 1cm) was obtained from SPI Supplies (West Chester, PA, USA). Glucose oxidase (GOx) from *Aspergillus niger*, glucose, 1-ethyl-3-(3-dimethylaminopropyl) carbodiimide (EDC), sulfo-N-hydroxysulfosuccinimide (sulfo-NHS), ferrocenecarboxylic acid (FCA), K_2HPO_4 and KH_2PO_4 were all purchased from Sigma-Aldrich (Oakville, ON, Canada). All solutions were prepared using Milli-Q water (resistivity ⩾ 18MΩ·cm).

3.2.2 Preparation of the Peptide-Modified HOPG Electrode

A freshly cleaved HOPG electrode was covered with 100μl of 0.5mg/ml EFK16-II stock solution and incubated overnight to have peptide modification on the graphite surface. The electrode surface was then washed with Milli-Q water three times to remove loosely attached EFK16-II.

3.2.3 Enzyme Immobilization on the Peptide-Modified HOPG Electrode

Two immobilization methods were used and compared in this study. In the first method[121], 100μl of 50mM potassium phosphate buffer (pH 5.5) containing 2mM EDC and 5mM sulfo-NHS was injected onto the EFK16-II modified HOPG electrode surface. The electrode was left for 1h to convert carboxylate groups of EFK16-II into their sulfo-NHS ester. The electrode was then washed with 100μl of 50mM potassium phosphate buffer (pH 5.5) three times and immediately covered with 100μl of 50mM potassium phosphate buffer (pH 5.5) containing 1mg/ml GOx, and

incubated overnight at 4°C. The enzyme electrode (Method 1 GOx electrode) was then rinsed with a potassium phosphate buffer (pH 7.0) and used immediately.

In the second method, 100µl of 50mM potassium phosphate buffer (pH 5.5) containing 2mM EDC, 5mM sulfo-NHS, 1mg/ml GOx was injected onto the peptide modified HOPG electrode surface and then incubated overnight at 4°C. The electrode (Method 2 GOx electrode) was then rinsed with a potassium phosphate buffer (pH 7.0) and used immediately. The second method is more convenient and more efficient in terms of GOx immobilization, which will be investigated in more detail in section 3.3.

3.2.4 Atomic Force Microscopy (AFM)

The structure of the peptide-modified HOPG surface was investigated by a PicoScan^{TM} AFM (Molecular Imaging, Phoenix, AZ). To prepare the AFM samples, 100µl of 0.5 mg/ml EFK16-II stock solution was injected onto a freshly cleaved HOPG surface and incubated for 3h. It was then washed 3 times with Milli-Q water and left dry for 1-2 h. Silicon crystal tips (type NCL, Nanosensors^{TM}) with a radius of 10nm were used for AFM tapping mode imaging. The AFM tip resonance frequency for imaging was between 160 and 180 kHz.

3.2.5 Attenuated Total Reflection Fourier Transform Infrared Spectroscopy (ATR-FTIR)

Attenuated total reflection fourier transform infrared spectroscopy measurements were carried out using a Tensor 27 FTIR microscope (Bruker Optics, Ltd.) with 2cm^{-1} resolution over the range of 600-2000cm^{-1}. Each spectrum presented in this study is the result of 500 repetitive scans.

3.2.6 Electrochemical Measurements

Electrochemical measurements were carried out in a conventional one-compartment cell with a CHI650A Potentiostat (CH Instruments Inc., Austin, TX) at ambient temperature (20±2°C). All potentials were measured against a Ag/AgCl reference electrode (Bioanalytical Systems, West Lafayette, IN), and the counter electrode was a platinum wire. All scans were started at the negative end of the potential range and proceeded in the positive direction. For the chronoamperometric experiments, a constant potential of +0.45mV against saturated Ag/AgCl was applied.

3.3 Results and Discussion

3.3.1 Self-assembly of EFK16-II on the HOPG electrode surface

Peptide self-assembly on the HOPG electrode surface was investigated by atomic force microscopy. Figure 3.2a and b show images of surfaces of a bare HOPG and an EFK16-II modified HOPG, respectively. Peptide nanofibres were observed on the EFK16-II-modified HOPG electrode. This structure is similar to what Yang at al.[122] observed in a study of the self-assembly of another ionic-complementary peptide EAK16-II (sequence: AEAEAKAK-AEAEAKAK) on HOPG surface. From Figure 3.2b, it can be seen that most of the HOPG surface was covered by EFK16-II nanofibres. One of the advantages of ionic-complementary peptide for surface modification is that the modification process is quite simple, involving only the immersion of the substrate in an aqueous peptide solution. The adsorption of EFK16-II on HOPG surface is likely due to hydrophobic interactions. The ionic-complementary peptide has an amphiphilic structure. As shown in Figure 3.1, the upper side residues of the peptide are hydrophilic and the lower side residues are hydrophobic. When in contact with a hydrophobic

surface (e.g. HOPG), the peptide tends to orient itself so that the hydrophobic residue phenylalanine will face the hydrophobic HOPG surface. On the other hand, the hydrophilic residues glutamic acid and lysine will face the opposite direction, which is towards the solution phase covering the HOPG surface. A high coverage of the peptide nanofibres and orientation of glutamic acid residues make EFK16-II-modified HOPG electrodes a perfect platform for enzyme immobilization.

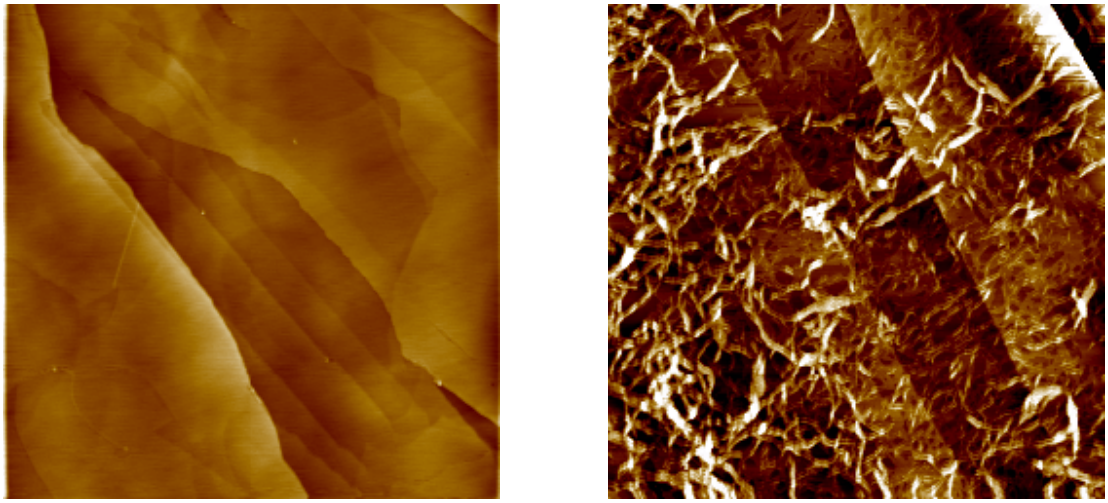

(a) (b)

Figure 3.2 Tapping mode AFM images of a bare HOPG surface (a) and EFK16-II modified HOPG surface (b). The scan scale is 6μm×6μm.

3.3.2 Chemistry in Enzyme Immobilization

Carboxyl groups of the glutamic acid residues on the ionic complementary peptide participate in enzyme immobilization. These were used to covalently link amine groups from GOx. Fewer available carboxyl groups on the HOPG electrode surface lead to less immobilized GOx. The

method introduced by Yang et al[121] (the first method) has the problem that carboxyl groups can be consumed by amine groups on nearby lysine residues in the peptide. After a carboxyl group is activated by forming a sulfo-NHS ester, which is susceptible to attack by amines, nearby amine groups from lysine residues of the peptide are likely to react with this ester and form an amide bond. Over a 1-hour activation period, the peptide side chains are likely to cross-link so that few carboxyl groups survive for enzyme immobilization. This process is shown in Figure 3.3a.

On the contrary, the second immobilization method, which is recommended in this study, inhibits peptide cross-linking by avoiding the activation period. A mixed solution of GOx, EDC and sulfo-NHS was injected onto the EFK16-II modified HOPG electrode surface directly. More active enzyme molecules can be immobilized onto the electrode surface because fewer peptide carboxyl groups react with amine groups of the peptide. In addition, GOx also has carboxyl groups on its surface; GOx carboxyls could be activated in the solution containing EDC and sulfo-NHS and react with amine groups of the peptide. This can also contribute to improved active GOx immobilization. The process is shown in Figure 3.3b.

The above ideas are supported by both FTIR results and electrochemical measurements.

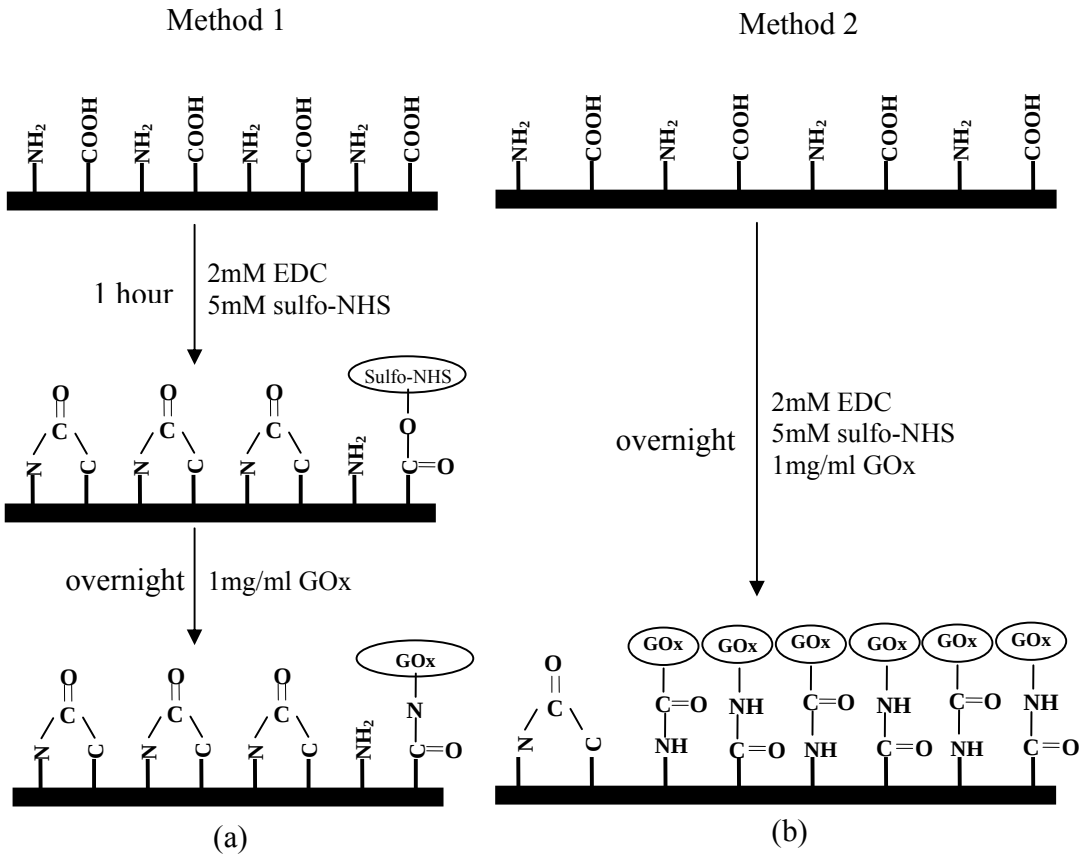

Figure 3.3 Schemes for enzyme immobilization: the black solid rectangles denote the EFK16-II modified HOPG electrode; (a) the EFK16-II modified HOPG electrode was activated by 2mM EDC and 5mM NHS for 1h, then it was covered by 1mg/ml GOx solution overnight; (b) the EFK16-II modified HOPG electrode was covered by 2mM EDC, 5mM sulfo-NHS, 1mg/ml GOx overnight

3.3.3 ATR-FTIR Spectra

The ATR-FTIR spectrum of self-assembled EFK16-II on the HOPG surface is presented in Figure 3.4(a). The peptide film was then covered by 100µl potassium buffer (pH 5.5) containing 2mM EDC and 5mM sulfo-NHS for 1h. After that, the surface was washed by Milli-Q water and dried for ATR-FTIR measurement. Results are shown in Figure 3.4(b), where a stronger intensity of the characteristic peak for the amide group is evident at 1550cm^{-1} [123]. This provides supporting evidence that the peptide was cross-linked during this period by forming amide bonds. Figure 3.4(a) shows the N-H deformation vibration peak at 840cm^{-1} and C-N stretching vibration peak at 1130cm^{-1} from primary amines of lysine. However, both of these peaks are absent in Figure 4.4(b), indicating consumption of amine groups due to peptide cross-linking.

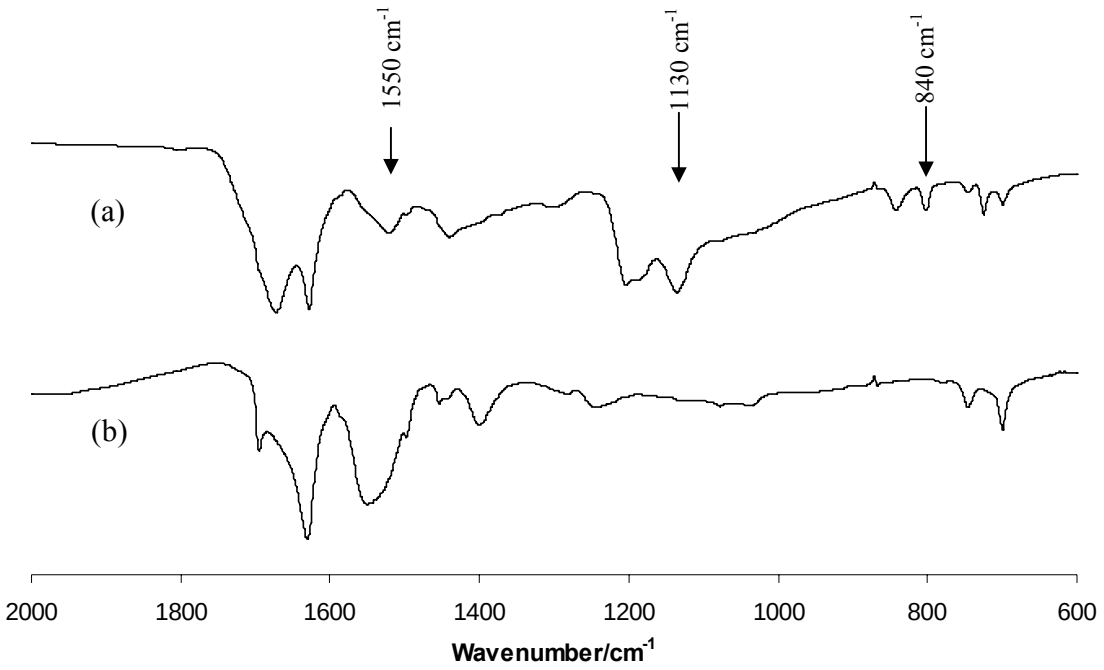

Figure 3.4 ATR-FTIR spectra of self-assembled EFK16-II on the HOPG surface (a) and cross-linked EFK16-II on the HOPG surface (b).

3.3.4 Electrochemical Comparison of Two Immobilization Methods

In order to compare the two methods for enzyme immobilization, electrochemical measurements were conducted. Figure 3.5 shows cyclic voltammograms of the GOx-immobilized EFK16-II modified HOPG electrode in 0.1M potassium phosphate buffer (pH 7.0) containing 0.2mM FCA as a mediator[124] in the absence and presence of 20mM glucose. In the absence of glucose (Figure 3.5a and b), similar CV curves were observed for both the Method 1 GOx electrode and Method 2 GOx electrode. In the presence of 20mM glucose (Figure 3.5c and d), the Method 2 GOx electrode produces an anodic peak current of 56.0μA while the Method 1 GOx electrode yields an anodic peak current of only 16.0μA. A much higher electrocatalytic current achieved by the Method 2 GOx electrode suggests that more active GOx molecules were immobilized on the electrode surface using the second method. During this immobilization process, more GOx molecules maintained their catalytic activity[125].

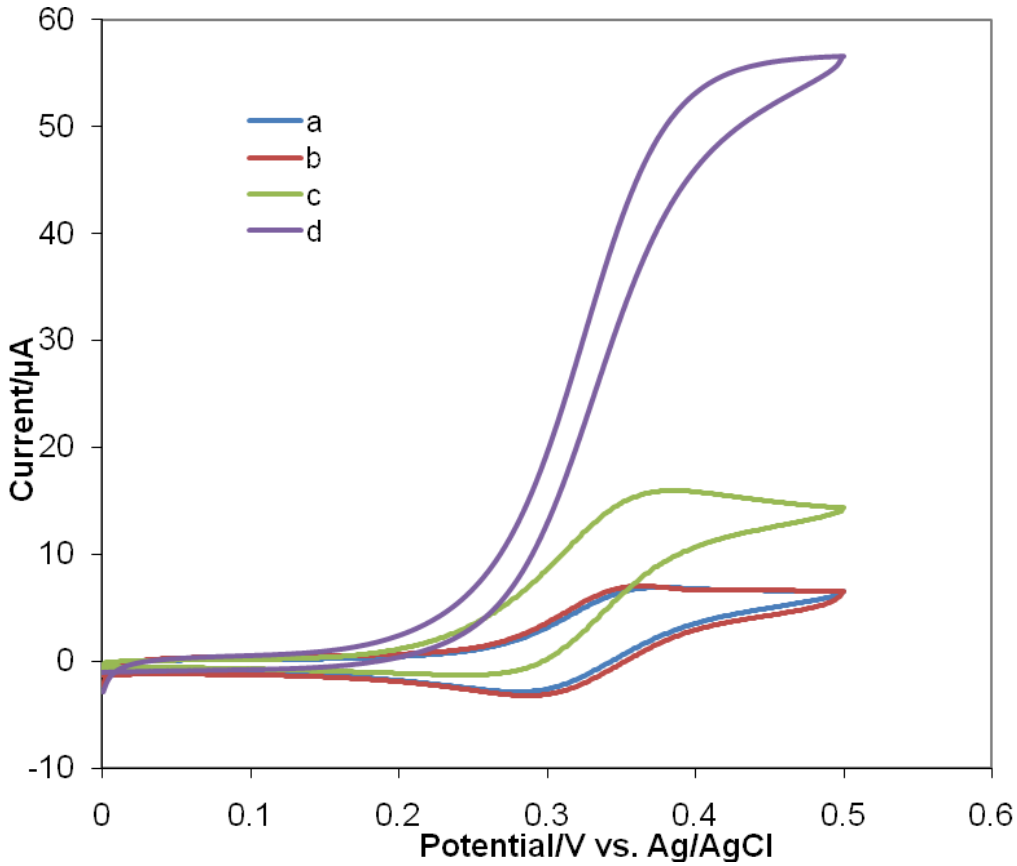

Figure 3.5 Cyclic voltammograms in 0.1M potassium phosphate buffer (pH 7.0) containing 0.2mM FCA: (a) Method 1 GOx electrode without glucose; (b) Method 2 GOx electrode without glucose; (c) Method 1 GOx electrode with 20mM glucose; (d) Method 2 GOx electrode with 20mM glucose. Scan rate is 2mV/s; electrode area is 1cm×1cm.

The performance of these two electrodes was also compared using chronoamerometry. I-t curves (Figure 3.6) for the enzyme electrodes were acquired at a constant potential of +0.45V vs. Ag/AgCl. Solutions with different concentrations of glucose containing 0.2mM FCA were used. For both Method 1 and Method 2 GOx electrodes, steady-state currents were obtained within

2min. The steady-state currents increased when the glucose concentration rose from low to high before leveling off at high concentration. This behavior is typical for enzyme modified electrodes [126]. The calibration curves shown in Figure 3.7a were obtained by subtracting the steady-state currents with background currents. The curves for both electrodes have a linear range up to 8mM glucose. The Method 2 GOx electrode has a sensitivity value of 4.94mA M^{-1} cm^{-2}, which is almost 6 times higher than that of Method 1 GOx electrode (0.84mA M^{-1} cm^{-2}). The current densities of the Method 1 and Method 2 GOx electrodes at 30mM glucose are 49.7μA cm^{-2} and 9.4μA cm^{-2}, respectively. The much higher current density for Method 2 GOx electrode is further support that more active GOx molecules were immobilized onto the EFK16-II modified HOPG electrode surface, when the second immobilization method was used.

Results from both sensitivity and saturated current data provide evidence for the hypothesis that the carbodiimide agent causes cross-linking between peptide residues, leading to fewer active GOx molecules immobilized.

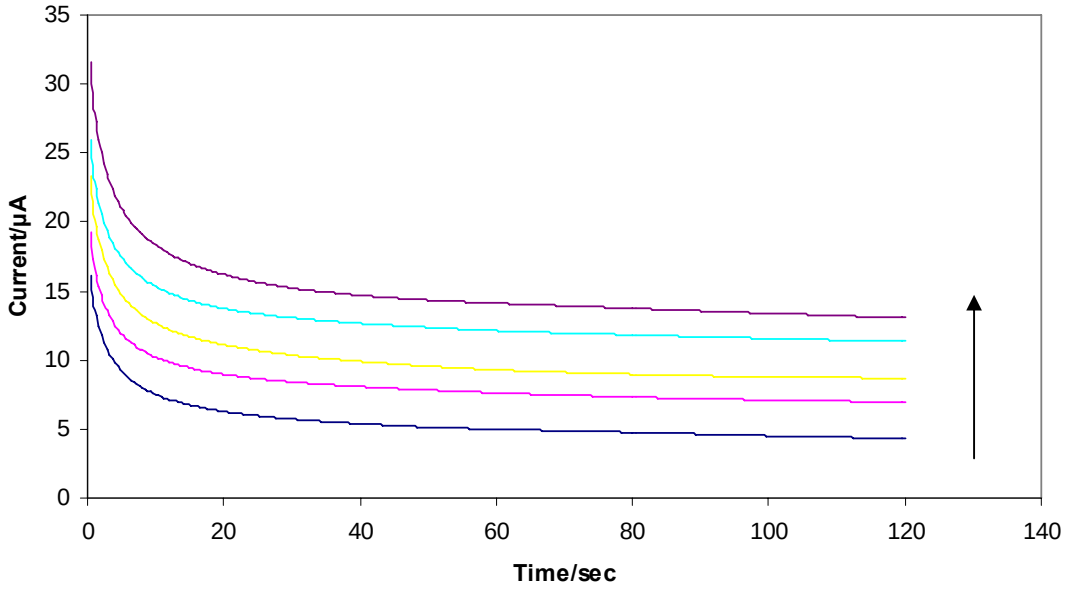

(a)

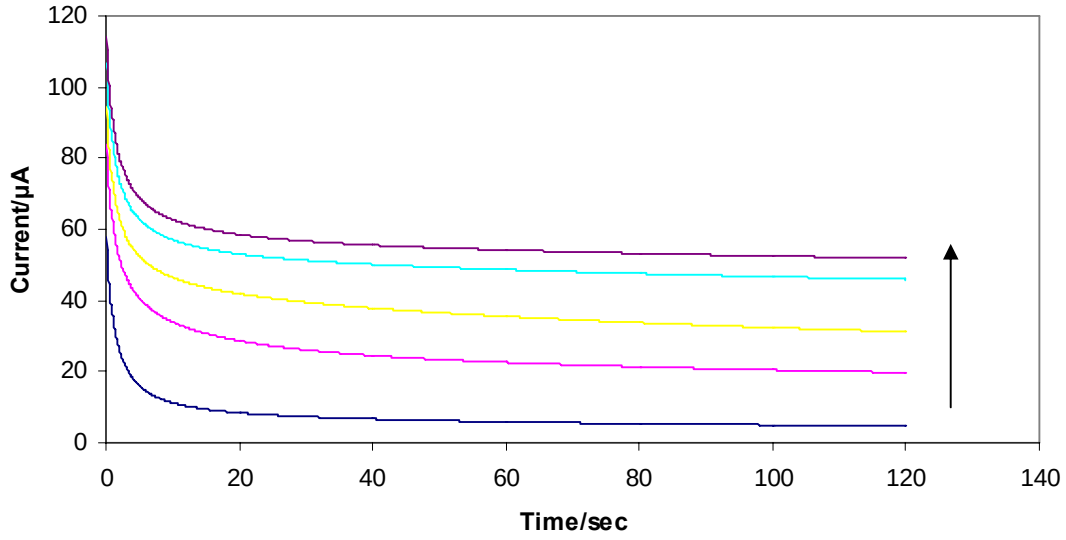

(b)

Figure 3.6 Chronoamperometric i-t curves of Method 1 GOx electrode (a) and Method 2 GOx electrode (b) in 0.1M potassium phosphate buffer (pH 7.0) containing 0.2mM FCA and various concentrations of glucose (from bottom to top, 0, 3, 5, 10, 20 mM). Electrode area is 1cm×1cm.

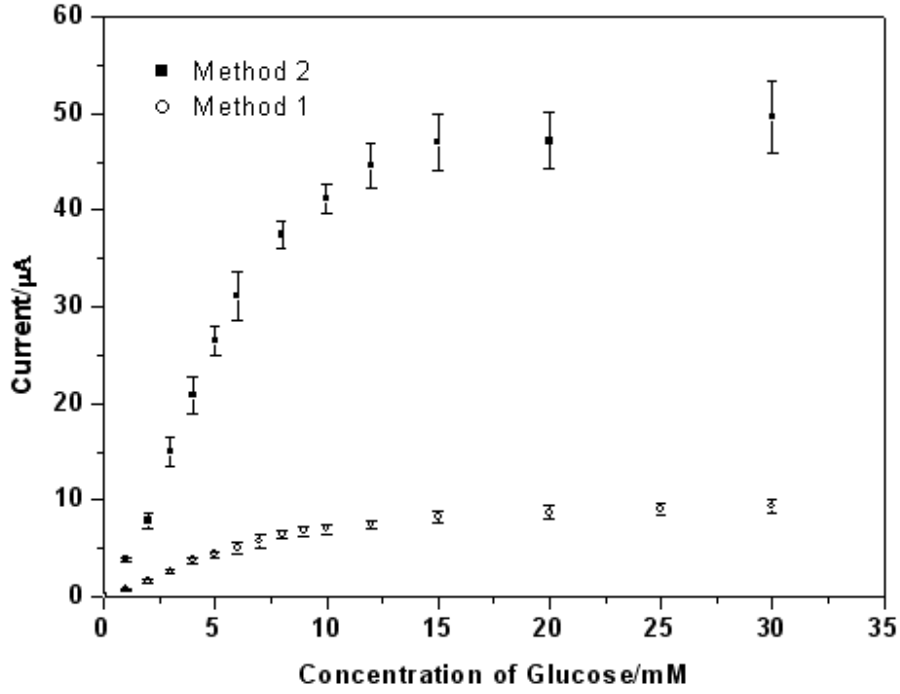

(a)

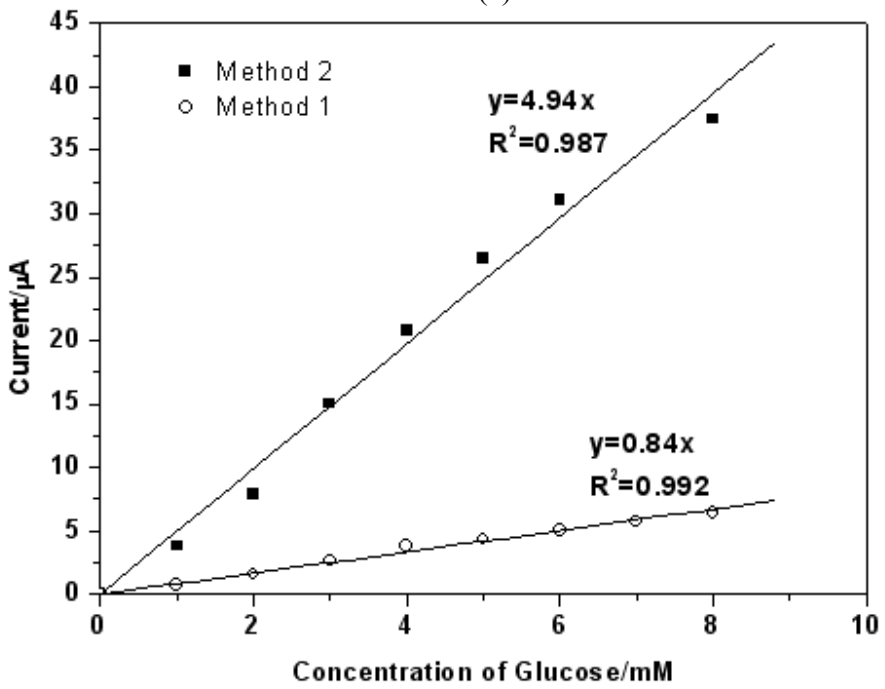

(b)

Figure 3.7 Calibration curves of Method 1 and 2 GOx electrodes (a) and linear range of the calibration curves (b).

The stabilities of both Method 1 and Method 2 GOx electrodes were investigated by comparing the anodic currents of cyclic voltammograms for 20mM glucose before and after one week of storage at 4°C in 100mM potassium phosphate buffer (pH 7.0). The Method 1 GOx electrode retained 86% of its original activity, while the Method 2 GOx electrode showed 81% of its original value. One possible reason for the good stabilities of these electrodes is that the ionic-complementary peptide modified HOPG electrodes provide a biocompatible environment for the enzyme.

The above results not only demonstrate a good method for enhanced active enzyme immobilization, but also provide insight into the appropriate design of peptide sequences for biosensor applications. Peptide self-assembly is important because this yields a stable structure on the HOPG electrode. Lysine residues play a significant role in EFK16-II self-assembly because of electrostatic attraction between lysine residues and glutamic acid residues[110]. On the other hand, lysine residues with amine groups appear to be detrimental in terms of enzyme immobilization, according to this study. A peptide that contains only carboxyl groups in the side chains and forms a stable nanostructure on the electrode surface would be an ideal candidate for biosensor applications.

3.4 Conclusions

The ionic-complementary peptide EFK16-II was used to modify an HOPG electrode, providing a nanofibre structure of the self-assembling peptide on the electrode surface. Carboxyl groups from glutamic acid residues were used for immobilization of GOx. However, we found in this study that amine groups from lysine residues of EFK16-II can also react with nearby carboxyl groups, forming intra- or interpeptide amide bonds and this affects subsequent enzyme

immobilization significantly. To overcome this problem, we introduced a simple and straightforward method for GOx immobilization. A mixed solution of GOx, EDC and sulfo-NHS was injected onto the surface of EFK16-II modified HOPG electrodes. This method inhibited cross-linking of the peptide itself and more active GOx molecules were immobilized. A much higher current density (49.7μA/cm^2 vs. 9.4μA/cm^2 at 30mM glucose) and sensitivity (4.94mA M^{-1} cm^{-2} vs. 0.84mA M^{-1} cm^{-2}) were achieved with this method. The greatly enhanced electrochemical performance makes the ionic-complementary peptide modified electrode a promising platform in biosensing applications.

Chapter 4 EAK16-II Modified HOPG Electrode in Biosensing Application

4.1 Introduction

With recent development of nano-bio materials, self-assembling peptides emerge as a new class of materials, which have many potential applications in biomedical and pharmaceutical areas. These peptides were first found by Zhang et al.[127,128] in 1992 from zoutin, a reported Z-DNA binding protein in yeast. The self-assembling peptides are biocompatible and biodegradable.[128] These properties make them ideal as matrices in tissue engineering and drug delivery.

Ionic-complementary peptides EAK16-II and RAD 16-II can self-assemble into well-ordered nanofibers and porous membranes, with fiber width of 10nm and pore size ranging from 5 to 200nm.[128,129] Their three-dimensional nanofiber structures are similar to natural extracelluar matrices such as collagen. These peptides have been used to study cell attachment, survival and proliferation.[130-132] The peptide scaffolds from RADA16-I and RADA16-II form nanofiber scaffolds in physiological solutions that stimulated extensive rat neurite growth, and active synapse formation on the peptide surface was successfully achieved.[133]

Peptides also show much potential for drug delivery. The most attractive aspect of peptide-mediated drug delivery is the natural propensities of many peptides for cell penetration and targeting.[134-136] As a result, many novel delivery systems involve peptides to achieve targeted delivery for anticancer therapeutics and to cross the cell membrane barrier for gene/siRNA delivery. In one study, the ionic-complementary peptides EAK16-II was shown to stabilize

pyrene microcrystals in an aqueous solution at concentration up to ten thousand times above its solubility in water of 7.0×10^{-7}M.[137] EAK16-II was investigated to stabilize a hydrophobic anticancer agent ellipticine in another study.[138] EAK16-II can stabilize two forms ellipticine, protonated or crystalline, depending on different combinations of EAK16-II and ellipticine concentrations. In addition, the complexes containing protonated ellipticine are found to have a better anticancer activity against two cancer cell lines, A549 and MCF-7.

Recently, self-assembled nanotubes of the peptide diphenylalanie (FF) have shown potential for use in biosensor applications.[75,76] Modification of carbon and gold electrodes by these peptide nanotubes can improve the reaction reversibility of the $Fe(CN)_6^{4-}/Fe(CN)_6^{3-}$ redox couple; it also enables these electrodes to exhibit a direct and unmediated response to H_2O_2 and NADH. In addition, glucose oxidase-based biosensors modified by such peptide nanotubes exhibited unmediated, rapid response to successive additions of glucose. In another study, an ionic-complementary peptide EFK16-II was used to modify a graphite electrode.[121] It was found that the peptide nanofiber coating did not block electron transfer to the electrode. Glucose oxidase could be immobilized onto the peptide nanofiber-modified electrode and used as a glucose sensor. The linear range between current and glucose concentration extends as far as 7mM.

In this study, another typical ionic-complementary peptide EAK16-II was investigated for biomolecular sensing. The molecular structure of EAK16-II is shown in figure 4.1. EAK16-II was used to modify a hydrophobic electrode, highly order pyrolytic graphite (HOPG). This EAK16-II modified HOPG electrode was characterized by atomic force microscopy (AFM). The redox couple $Fe(CN)_6^{3-/4-}$ was used as a probe to test the electrochemical properties of the modified electrode. This electrode was then further studied in immobilizing different compounds, including glucose oxidase (GOx), ferrocene carboxylic acid (FCA) and myoglobin (Mb). This

work provides insights into applications of ionic-complementary peptides in bioelectro-analysis.

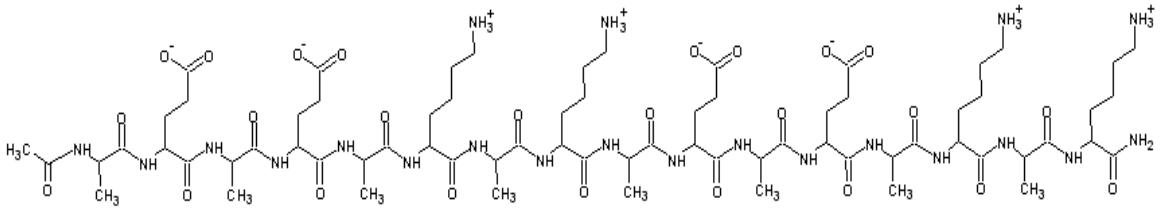

Figure 4.1 Molecular structure of EAK16-II (AEAEAKAKAEAEAKAK)

4.2 Materials and Methods

4.2.1 Materials

The ionic-complementary peptide AEAEAKAKAEAEAKAK (EAK16-II) was purchased from CanPeptide Inc. (Quebec, Canada) and used without further purification. In the peptide sequence, F stands for phenylalanine, E stands for glutamic acid and K stands for lysine. The N-terminus and C-terminus of the peptide were protected by acetyl and amino groups, respectively.

Highly ordered pyrolytic graphite (HOPG, 1cm × 1cm) was obtained from SPI Supplies (West Chester, PA, USA). Glucose oxidase (GOx) from *Aspergillus niger*, glucose, 1-ethyl-3-(3-dimethylaminopropyl) carbodiimide (EDC), sulfo-N-hydroxysulfosuccinimide (sulfo-NHS), ferrocenecarboxylic acid (FCA), K_2HPO_4, KH_2PO_4 and Cytochrome *c* (Cyt *c*) were all purchased from Sigma-Aldrich (Oakville, ON, Canada). All solutions were prepared using Milli-Q water (resistivity≥18MΩ·cm).

4.2.2 Preparation of the Peptide Modified HOPG Electrode

A freshly cleaved HOPG electrode was covered with 100µl of 0.2mg/ml EAK16-II stock solution and incubated overnight to modify the graphite surface. The electrode surface was then washed by Milli-Q water three times to remove loosely attached EFK16-II. The EAK16-II-modified HOPG electrode was then further modified as described in the following sections.

4.2.3 Atomic Force Microscopy

The structure of the peptide-modified HOPG surface was investigated using a PicoScan^{TM} AFM (Molecular Imaging, Phoenix, AZ). To prepare the AFM samples, 100µl of 0.5 mg/ml EFK16-II stock solution was injected onto a freshly cleaved HOPG surface and incubated for 3h. It was then washed 3 times with Milli-Q water and left dry for 1-2 h. Silicon crystal tips (type NCL, Nanosensors^{TM}) with a radius of 10nm were used for AFM tapping mode imaging. The AFM tip resonance frequency for imaging was between 160 and 180 kHz.

4.2.4 Electrochemical Measurements

Electrochemical measurements were carried out in a conventional one-compartment cell with a CHI650A Potentiostat (CH Instruments Inc., Austin, TX) at ambient temperature (20±2°C). All potentials were measured against a Ag/AgCl reference electrode (Bioanalytical Systems, West Lafayette, IN), while the counter electrode was a platinum wire. All scans were started at the negative end of the potential range and proceeded in the positive direction. For the chronoamperometric experiments, a constant potential of +0.45mV against saturated Ag/AgCl was applied.

4.3 Results and Discussion

4.3.1 Characterization of EAK16-II Modified HOPG Electrode

Self-assembly of EAK16-II on the HOPG electrode surface

Peptide self-assembly on the HOPG electrode surface was investigated by atomic force microscopy (AFM). Figure 4.2a and b show images of surfaces of a bare HOPG and an EAK16-II modified HOPG, respectively. Peptide nanofibers were observed on the EAK16-II modified electrode. Interestingly, these fibers were arranged in parallel or at 60º or 120º to each other. This phenomenon agrees with what Yang et al. observed.[122] The formation process has been characterized as being surface directed/assisted assembly. Such orientations of the adsorbed molecules/nanofibers arise presumably due to the hexagonal crystal structure of the HOPG (0001) surface and reflect the importance of substrate-peptide interactions.[122]

EAK16-II molecules have an amphiphilic structure. Thus, the adsorption of these molecules onto HOPG surface is likely due to hydrophobic interactions, similar to what was discussed in 3.3.1. The hydrophobic residues alanine faces the hydrophobic HOPG surface while the hydrophilic residues glutamic acid and lysine residues are oriented toward the solution covering the HOPG surface. A rich source of functional groups makes this EAK16-II modified HOPG electrode a good platform for various biosensing applications.

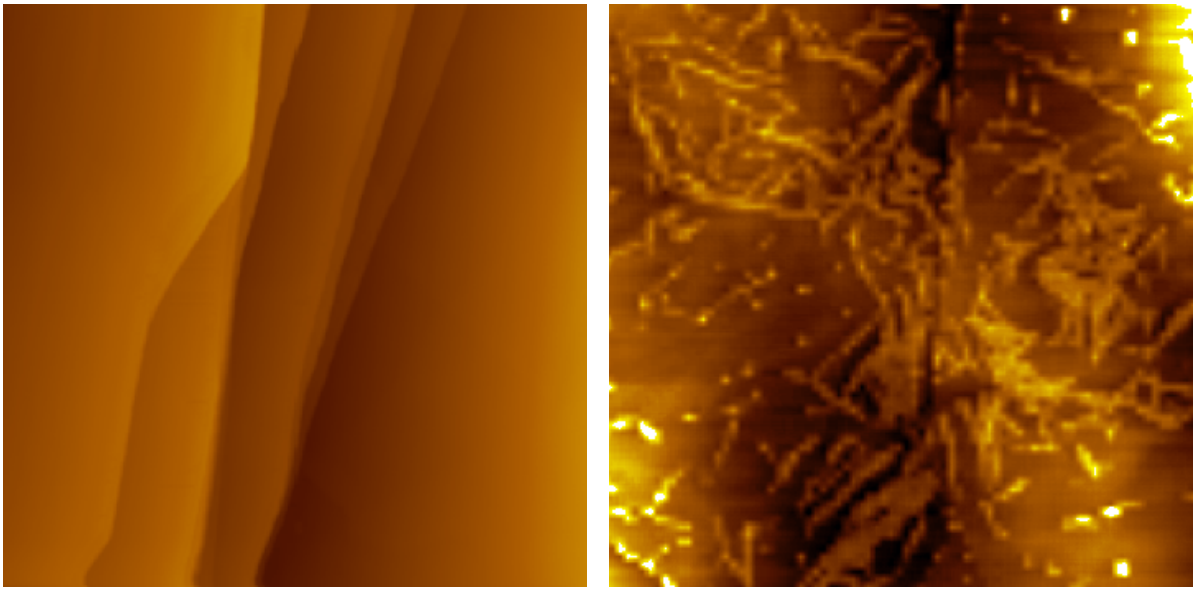

(a) (b)

Figure 4.2 Tapping mode AFM images of a bare HOPG surface (a) and EAK16-II modified HOPG surface (b). The scan area is 2μm×2μm.

Electrochemical characterization of the EAK16-II modified HOPG electrode

The electrochemical properties of EAK16-II modified HOPG electrode were studied by both cyclic voltammetry (CV) and electrochemical impedance spectroscopy (EIS) in a solution containing 1.0mM $K_3Fe(CN)_6/K_4Fe(CN)_6$ (1:1). CV is the most common and direct method to characterize an electrode. The cyclic voltammograms are shown in Figure 4.3. The peak separation ΔE_p ($\Delta E_p=E_{pa}-E_{pc}$) increased from 92mV for the unmodified electrode to 156mV for the EAK16-II modified electrode. An increase in the peak separation indicates that the $Fe(CN)_6^{3-}$ /$Fe(CN)_6^{4-}$ redox couple has become less reversible when the electrode is modified. In addition, both anodic and cathodic peak currents slightly decreased upon modification of the electrode. The result indicates that after immobilization by EAK16-II, the redox reaction rate of $Fe(CN)_6^{3-/4-}$

at the electrode is reduced slightly. The EAK16-II assembly on the surface slows down the electron transfer rate of the $Fe(CN)_6^{3-/4-}$ redox couple.

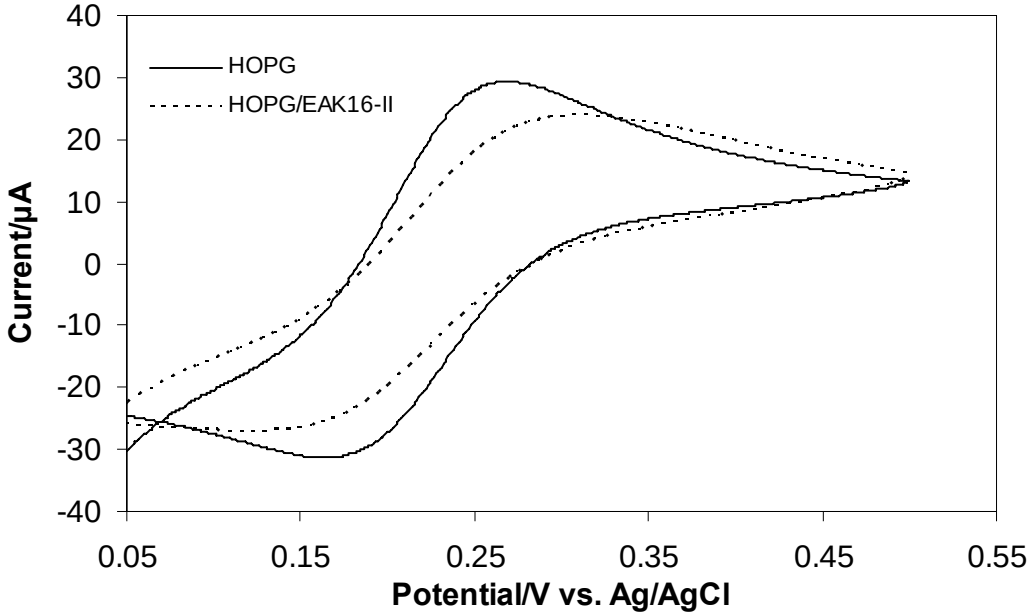

Figure 4.3 Cyclic voltammograms obtained in the presence of 1.0mM $K_3Fe(CN)_6/K_4Fe(CN)_6$ (1:1) with 0.1M KCl solution on bare HOPG (solid line) and EAK16-II modified HOPG (solid) electrodes at a scan speed of 2mV/s.

To further investigate the modification of EAK16-II on the HOPG surface, the impedance changes of HOPG and EAK16-II modified HOPG electrode have been studied using electrochemical impedance spectroscopy (EIS) in the presence of equimolar $Fe(CN)_6^{3-/4-}$ (Figure 4.4). To understand clearly the electrochemical properties of the electrode/solution interfaces, the Randle's equivalent circuit (inset of Figure 4.4) was chosen to fit the obtained impedance data.[139] In Randle's circuit, it is assumed that the resistance to charge transfer (R_{ct}) and the diffusion impedance (W) are both in parallel to the interfacial capacity (C_{dl}). This parallel combination of R_{ct} and C_{dl} gives rise to a semicircle complex plane plot of –Z" against Z'. The semicircle

diameter equals the charge transfer resistance (R_{ct}). This resistance exhibits the electron transfer kinetics of the redox-probe at the electrode interface. When HOPG is modified by EAK16-II, the diameter of the semicircle increases, indicating the EAK16-II layer hinders the charge transfer. This also proves that EAK16-II has been modified onto the HOPG surface.

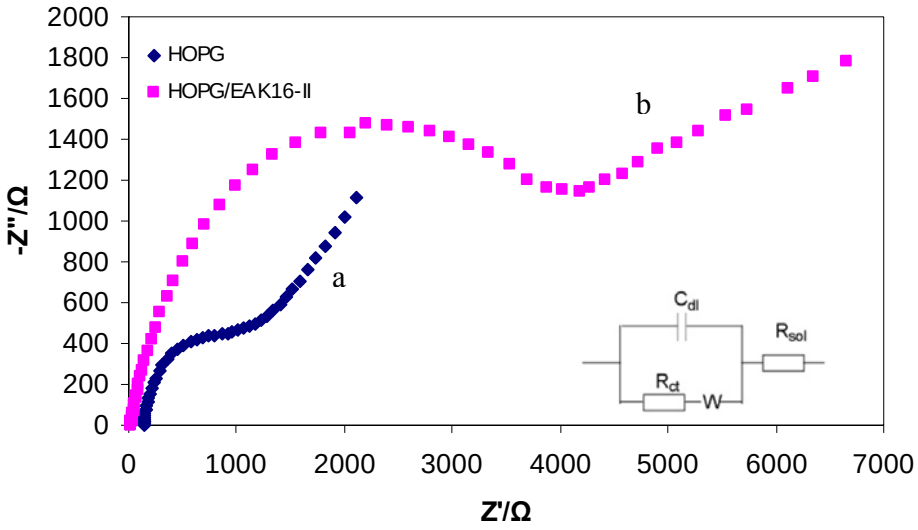

Figure 4.4 Electrochemical impedance spectroscopy of bare HOPG (curve a) and EAK16-II modified HOPG electrode (curve b) in the presence of 1.0mM $Fe(CN)_6^{3-/4-}$ containing 0.1M KCl as supporting electrolyte. Inset is the Randle's equivalent circuit. The electrode area is 1cm×1cm.

4.3.2 Application of EAK16-II Modified HOPG Electrode in Glucose Sensing

4.3.2.1 Effect of EAK16-II in Glucose Oxidase (GOx) Immobilization

In order to investigate the effect of EAK16-II in glucose oxidase (GOx) immobilization, four electrodes were prepared. The first electorde is bare HOPG electrode. The second electrode is prepared by covering 100µl 1mg/ml GOx on the surface of HOPG and incubating overnight at 4ºC (HOPG/GOx). The third electrode is prepared by covering 100µl 1mg/ml GOx on the

EAK16-II modified HOPG electrode and incubating overnight at 4ºC (HOPG/EAK16-II/GOx). The fourth electrode is prepared by activating the EAK16-II modified HOPG with 100µl 50mM potassium phosphate buffer (pH 5.5) containing 2mM EDC and 5mM sulfo-NHS for 1h at room temperature. This step converts the carboxyl groups into their NHS esters, which is susceptible to be attached by amines (Figure 4.5). GOx molecules are then covalently linked to the electrode surface by covering 100µl 1mg/ml GOx on this activated surface and incubating overnight at 4ºC (HOPG/EAK16-II-NH-GOx). All electrodes are washed with Milli-Q water to avoid loosely attached molecules.

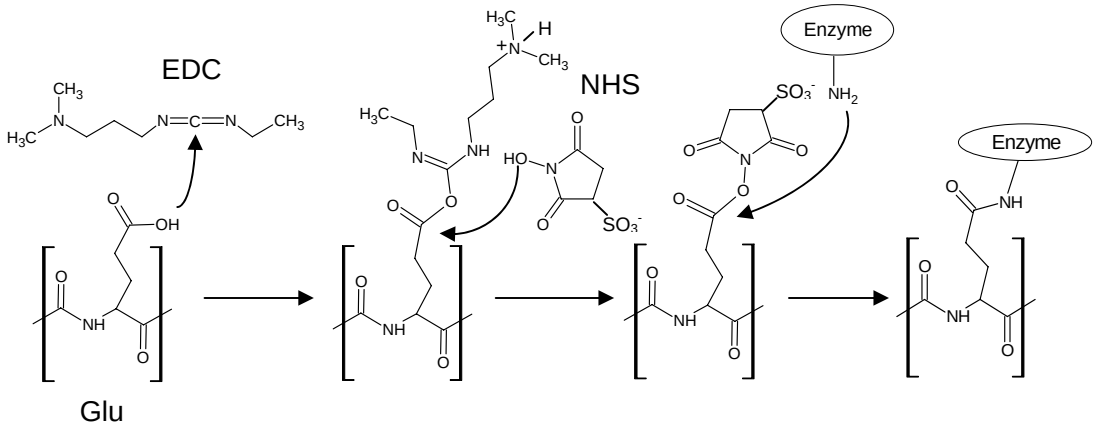

Figure 4.5 Covalent attachment of the enzyme GOx to the glutamic acid residue of EAK16-II using 1-ethyl-3-(3-dimethylaminopropyl) carbodiimide (EDC) and n-hydroxysulfosuccinimide (NHS)

Cyclic voltammetry of these four electrodes was conducted in the 100mM potassium phosphate buffer (pH 7.0) containing 0.2mM ferrocenecarboxylic acid (FCA) without (Figure 4.6a) and with 20mM glucose (Figure 4.6b). Without glucose, the voltammograms of these four electrodes are very similar, indicating that the electron transfer of FCA at the surface of these

four electrodes behaves similarly, although bare HOPG exhibits slightly higher redox peak currents. After adding 20mM glucose into the electrolyte, the anodic peak current on bare HOPG does not change, since there is no enzyme in this system. The fourth electrode, which has GOx molecules covalently linked to EAK16-II modified HOPG, shows the highest anodic peak current, indicating that the active enzyme molecules have been efficiently immobilized onto the electrode surface by covalent bonding. The enzyme molecules also retain their bio-catalytic activity, presumably due to the biocompatibility of the EAK16-II modified HOPG electrode. The third electrode, which has GOx molecules physically adsorbed on EAK16-II modified HOPG electrode, only has a slightly higher anodic peak current than that of the second electrode, GOx molecules physically adsorbed to HOPG. There may be two possible reasons. Firstly, GOx molecules have a higher affinity toward EAK16-II than HOPG, so that more GOx molecules are adsorbed. Secondly, since EAK16-II provides a biocompatible environment, more of the adsorbed enzyme molecules on the third electrode retain bio-catalytic activity.

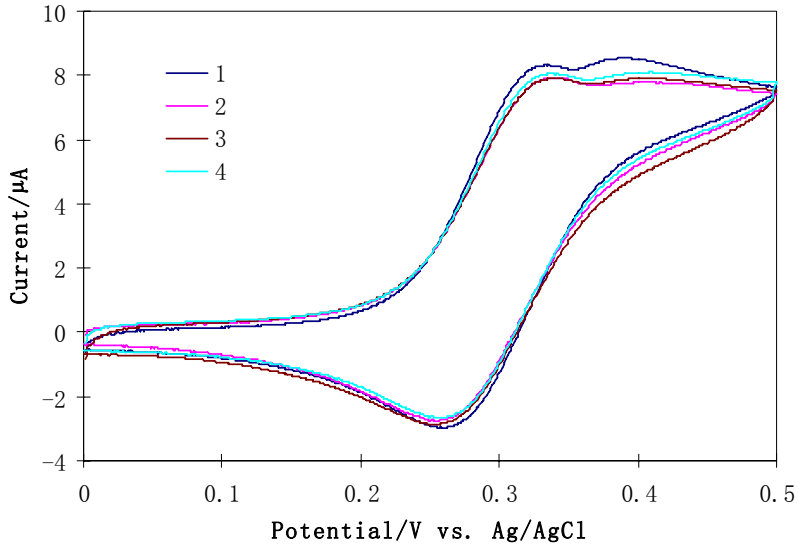

(a)

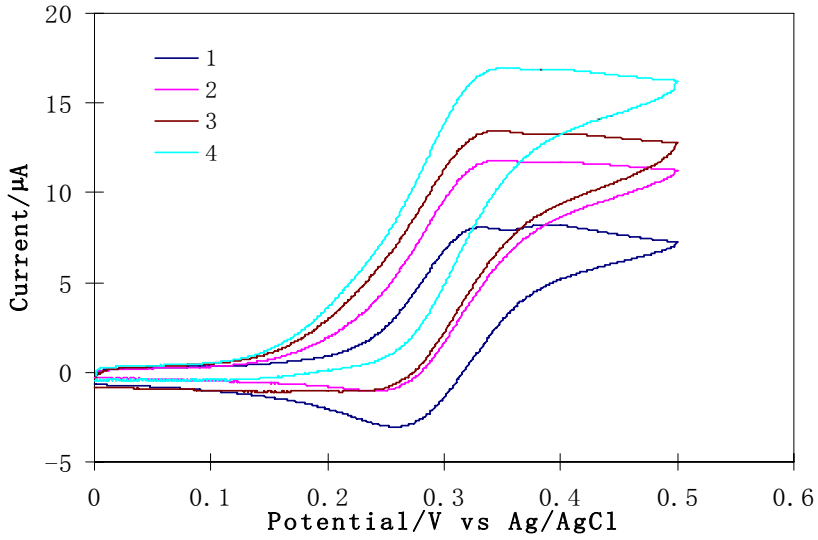

(b)

Figure 4.6 Cyclic voltammograms of four electrodes (1: HOPG; 2: HOPG/GOx; 3: HOPG/EAK16-II/GOx; 4: HOPG/EAK16-II-NH-GOx) obtained in the 100mM potassium phosphate buffer (pH 7.0) containing 0.2mM ferrocenecarboxylic acid (FCA) without (a) and with 20mM glucose (b). Scan speed is 2mV/s. Electrode area is 1cm×1cm.

4.3.2.2 Effect of Intro-/interpeptide Crosslinking

Similar to what is discussed in Chapter 3, the effect of intro-/interpeptide crosslinking of EAK16-II has also been investigated. Two electrodes were prepared for this purpose. The first electrode was prepared in the same way as the fourth electrode described in the previous section. It is called Method 1 GOx electrode here. The second electrode was prepared by covering 100µl 50mM potassium phosphate buffer (pH 5.5) containing 2mM EDC, 5mM sulfo-NHS and 1mg/ml GOx and incubating overnight at 4ºC. It is called Method 2 GOx electrode in this study. The chemistry involved is discussed in more detail in Chapter 3 and shown in Figure 4.7. It was shown in Chapter 3 that amine groups from lysine residues and carboxylic groups from glutamic acid residues can form amide bond under the addition of EDC and sulfo-NHS. The same intro-/interpeptide crosslinking reaction may also occur in the EAK16-II-modified HOPG electrode system. In order to explore this question, Method 1 and Method 2 GOx electrodes are prepared and studied using both cyclic voltammetry and chronoamperometry.

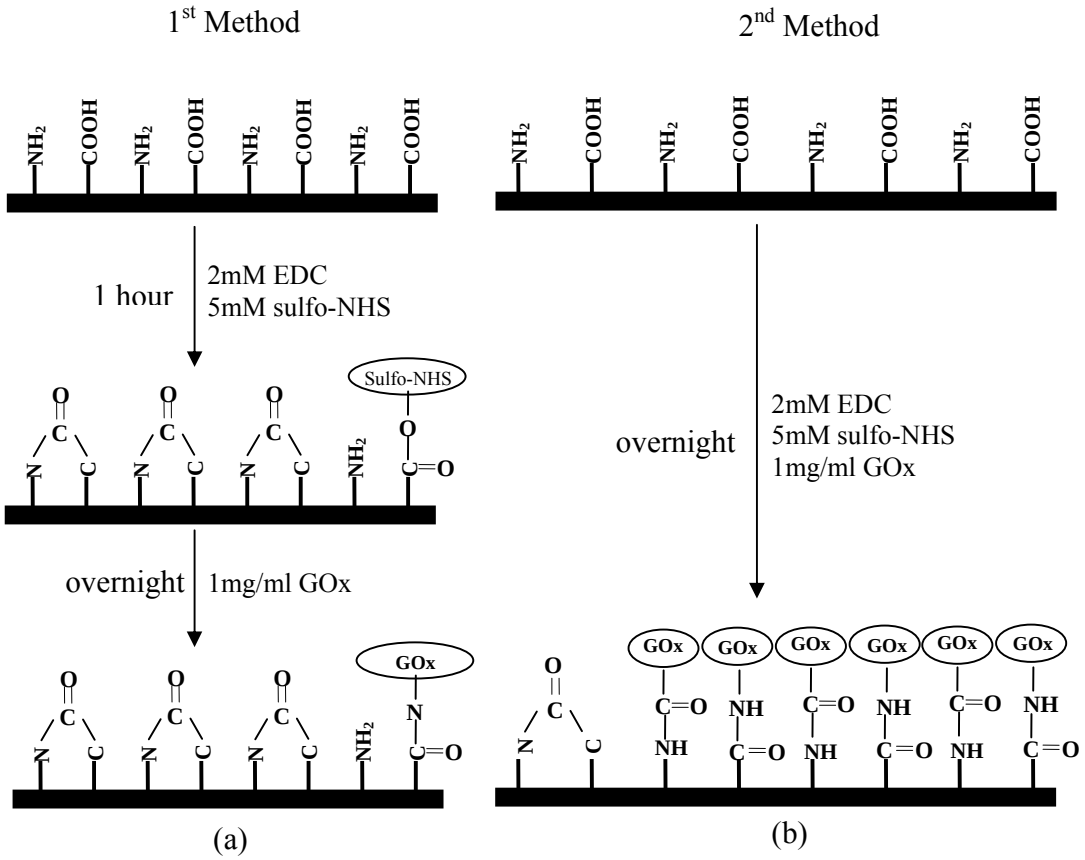

Figure 4.7 Schemes for enzyme immobilization: the black solid rectangles denote the EAK16-II modified HOPG electrode; (a) the EAK16-II modified HOPG electrode was activated by 2mM EDC and 5mM NHS for 1h, then it was covered by 1mg/ml GOx solution overnight; (b) the EAK16-II modified HOPG electrode was covered by 2mM EDC, 5mM sulfo-NHS, 1mg/ml GOx overnight.

The cyclic voltammograms in both cases were obtained in 100mM potassium phosphate buffer (pH 7.0) containing 0.2M FCA as the mediator in the presence of 20mM glucose and shown in Figure 4.8. It is quite obvious that the anodic peak current obtained with the Method 2 GOx electrode is much higher than that of Method 1 GOx electrode, indicating that more active GOx molecules were immobilized onto the electrode surface using the second method. This is same as the situation with the EFK16-I- modified GOx electrode.

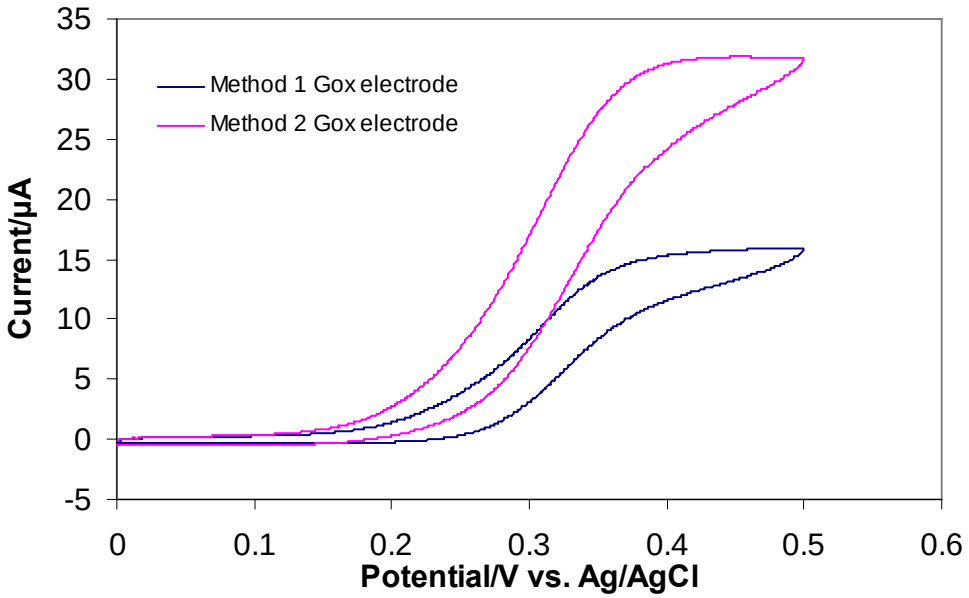

Figure 4.8 Cyclic voltammograms in 0.1M potassium phosphare buffer (pH 7.0) containing 0.2mM FCA and 20mM glucose of Method 1 GOx electrode (blue line) and Method 2 GOx electrode (purple line). Scan rate is 2mV/s; electrode area is 1cm×1cm.

The performance of these two electrodes was also compared by chronoamperometry. I-t curves (Figure 4.9a and b) of the enzyme electrodes were acquired at a constant potential of 0.45V against the Ag/AgCl reference electrode. Different concentrations of glucose solution containing 0.2mM FCA as the mediator were used. For both the Method 1 and Method 2 GOx electrodes,

steady-state current was obtained within 2min. The steady-state currents increased as the glucose concentration rose from low to high before levelling off at high glucose concentration. This is typical for enzyme-modified electrodes.

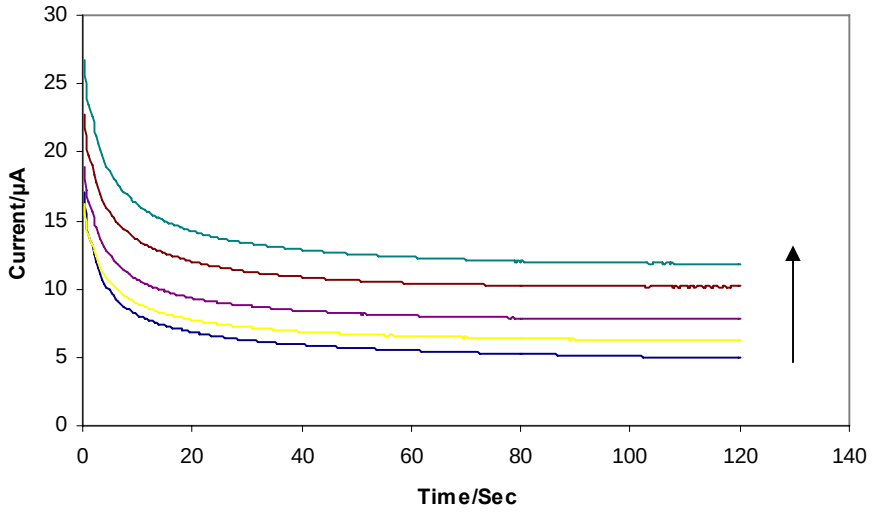

(a)

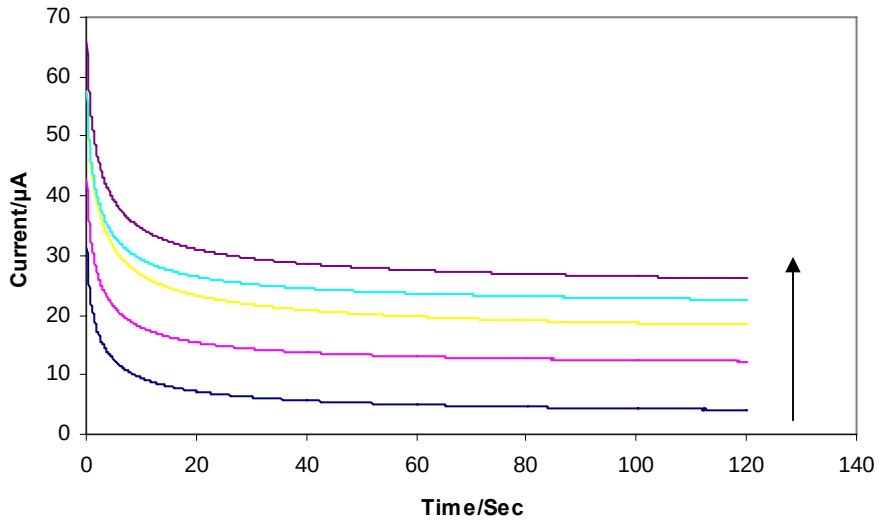

(b)

Figure 4.9 Chronoamperometric i-t curves of Method 1 GOx electrode (a) and Method 2 GOx electrode (b) in 0.1M potassium phosphate buffer (pH 7.0) containing 0.2mM FCA and various concentrations of glucose (from bottom to top, 0, 3, 5, 10, 20 mM). Electrode area is 1cm×1cm.

The calibration curves shown in Figure 4.10a were obtained by subtracting the steady-state currents with background currents. The curves for both electrodes have a linear range up to 8mM glucose. Method 2 GOx electrode has a sensitivity value of 2.4mA $M^{-1}cm^{-2}$, which is 4.5 times higher than that of Method 1 GOx electrode (0.53mA $M^{-1}cm^{-2}$). The current densities of Method 1 GOx electrode and Method 2 GOx electrode at 30mM glucose were 7.9μA cm^{-2} and 22.5μA cm^{-2}, respectively. The much higher current density for Method 2 GOx electrode is a direct indication that more GOx molecules were immobilized onto the EAK16-II modified HOPG electrode surface when using the second immobilization method.

From comparison of results from Chapter 3 and results reported here, it can be concluded that ionic-complementary peptides such as EFK16-II and EAK16-II, can cross-link either intro- or intermolecularly after they have self-assembled on a hydrophobic surface, for example, HOPG. Prevention of this crosslinking helps preserve functional groups for biomolecular immobilization.

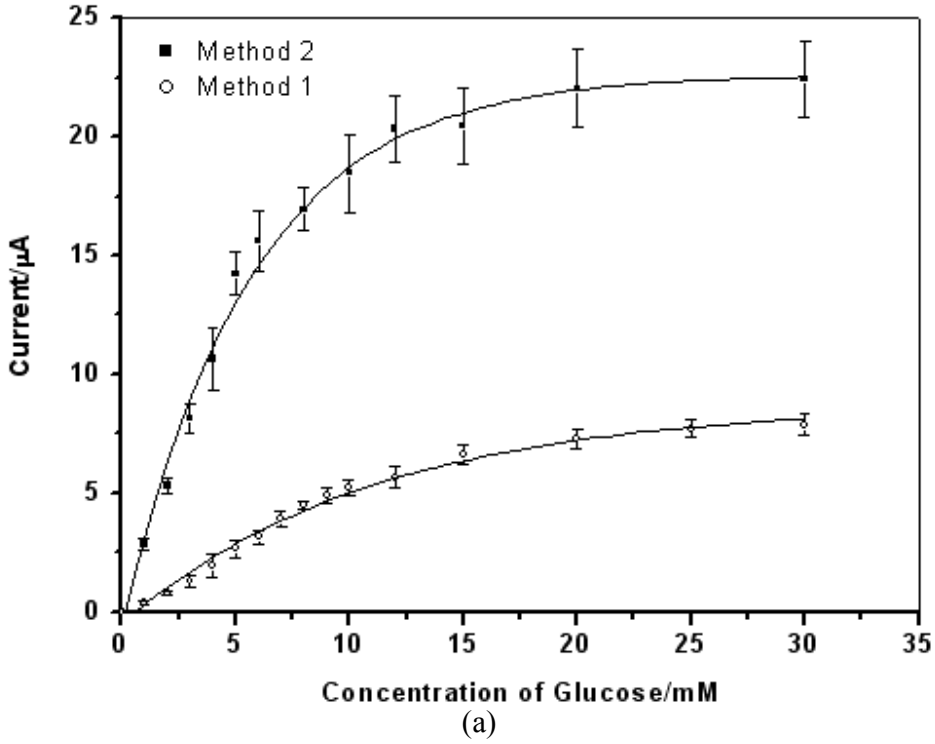

(a)

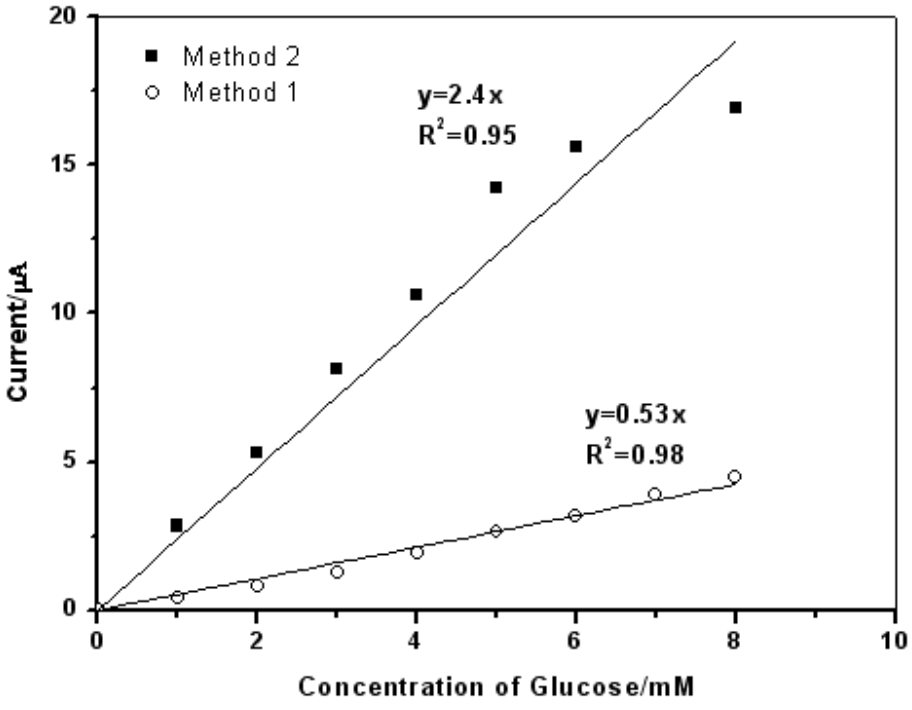

(b)

Figure 4.10 Calibration curves of Method 1 and Method 2 GOx eletrodes (a) and linear range of the calibration curves (b).

4.3.2.3 Acetylation Effect of Amine Groups of Lysine Residues

The results in the previous sections indicate that amine groups from lysine residues are detrimental for GOx immobilization. This is due to the reaction between amine and carboxyl groups. If amine groups are protected through some organic chemistry, this problem should be overcome. In light of this analysis, amine groups were acetylated before GOx immobilization. The electrode was prepared by the following procedures. After the HOPG electrode was immobilized by EAK16-II, this electrode was totally dried and 500µl 10% acetic anhydride in CH_2Cl_2 was injected onto the electrode surface. After 20min at room temperature, the acetic solution was removed by Kimwipes. The electrode was rinsed thoroughly by Milli-Q water. Then, 100µl 50mM potassium phosphate buffer (pH 5.5) containing 2mM EDC and 5mM NHS was injected onto the HOPG electrode surface and incubated at room temperature for 1h. At last, the modified electrode was rinsed by Milli-Q water and 100µl 100mM potassium phosphate buffer (pH 7.0) containing 1.0mg/ml GOx was injected onto the electrode surface and incubated at 4ºC overnight. Another electrode was prepared in the same way without acetylation.

Cyclic voltammetry was conducted in 100mM potassium phosphate buffer (pH 7.0) containing 0.2mM FCA and 20mM glucose. The result was shown in Figure 4.11. It can be observed that the acetylated electrode has a decreased anodic peak current compared with unacetylated electrode.

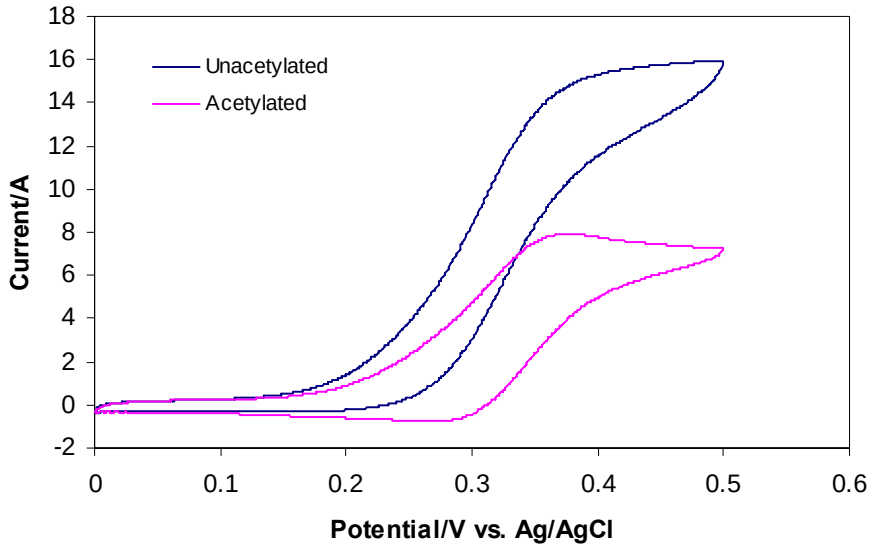

Figure 4.11 Cyclic voltammograms of acetylated and unacetylated electrodes in 100mM potassium phosphate buffer (pH 7.0) containing 0.2mM FCA and 20mM glucose. Scan rate is 2mV/s. The electrode area is 1cm×1cm.

In order to further characterize the electrode, chronoamperometry measurements were also conducted (Figure 4.12). The sensitivity for unacetylated electrode is 0.53 mA $M^{-1}cm^{-2}$ while that for acetylated electrode is 0.21 mA $M^{-1}cm^{-2}$. Both cyclic voltammetry and chronoamperometry results indicate that the acetylation process does not help to increase the immobilization of active GOx molecules. However, this is unexpected from the previous analysis. One possible reason for that is the ionic-complementary peptide, which is immobilized on the HOPG surface, may diffuse into the CH_2Cl_2 during the acetylation process. In this way, less peptide molecules are immobilized and consequently less GOx molecules can attached afterwards.

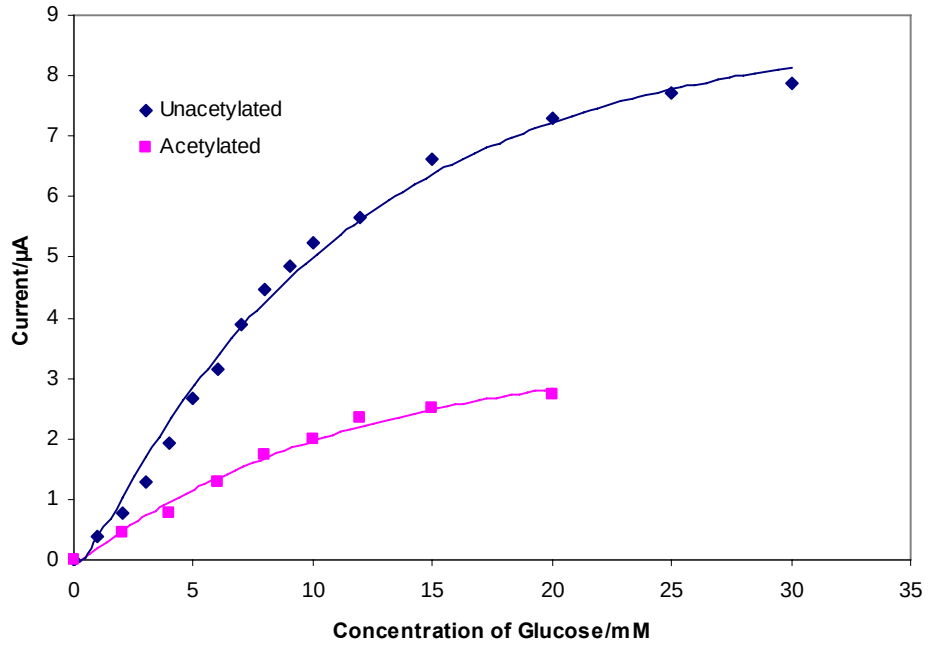

(a)

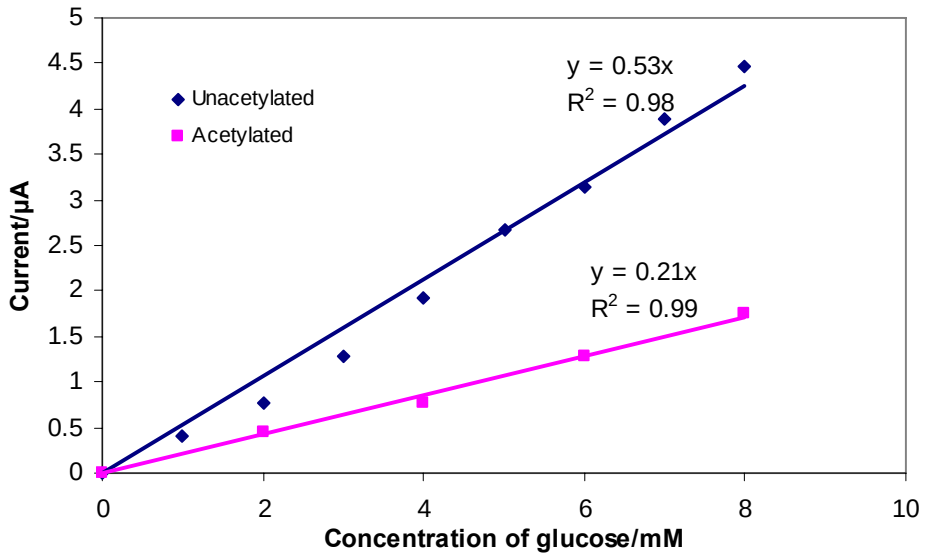

(b)

Figure 4.12 Calibration curves of enzyme electrode with acetylated and unacetylated EAK16-II (a) and linear range of the calibration curves (b). The applied potential is +0.45V vs. Ag/AgCl. The electrode area is 1cm×1cm.

4.3.3 Immobilization of Ferrocene Carboxylic Acid (FCA) onto EAK16-II Modified HOPG Electrode

Co-immobilization of enzymes and redox mediators onto electrode surfaces has received considerable attention.[30,118,140,141] In this context, Koid and Yokoyama[62] have electrochemically characterized an enzyme (GOx) electrode based on a ferrocene containing redox polymer. This redox polymer was based on cross-linked polyallylamine with covalently attached ferrocene. Such a ferrocene-containing cross-linked polyallylamine has been shown in Figure 4.13.

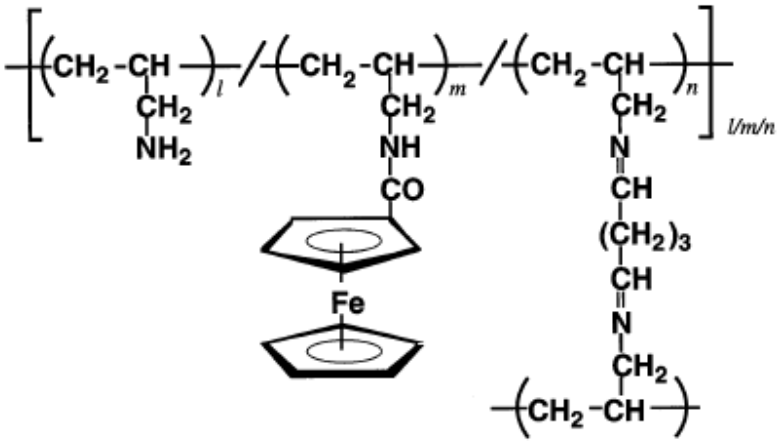

Figure 4.13 Ferrocene containing cross-linked polyallylamine[62]

This study of immobilizing redox mediator onto the polymer backbone encouraged us to pursue the application of ionic-complementary peptide in a similar way. As can be seen from Figure 4.1, the peptide, EAK16-II, has both amine groups and carboxyl groups on the backbone. The amine groups can be used to immobilize the mediator, such as ferrocene carboxylic acid (FCA), while the carboxyl groups can be used to immobilize the enzyme. A reagentless biosensor can be constructed in this way.

In order to test this idea, FCA was immobilized onto the EAK16-II modified HOPG electrode. Enough FCA was dissolved in 50mM potassium phosphate buffer (pH 5.5) to obtain a saturated solution. The saturated FCA solution was then activated by 2mM EDC and 5mM sulfo-NHS in order to transform the carboxyl groups into their sulfo-NHS esters, which are easy to react with amine groups to form amid bonds. 100µl of this activated FCA solution was then injected onto the EAK16-II modified HOPG electrode and incubated overnight at 4ºC. The electrode was thoroughly washed with pH 7.0 potassium phosphate buffer before conducting the electrochemical experiments. Cyclic voltammetry was done using this electrode as the working electrode. The result is shown in Figure 4.15. It can be seen that the redox current of immobilized FCA decreased dramatically when continually scanning over the range of 0-0.5V. The redox peak almost disappeared after 50 cycles at the rate of 50mV/s. This could be due to two possible reasons. First is that although the FCA was immobilized at first, it detached from the electrode gradually when a potential is applied at the electrode surface. Second, FCA may be not stable in this condition. FCA may decompose during this experiment.

Although it might be a good idea to immobilize the mediator onto the electrode along with the enzyme, it was not successful with the EAK16-II modified HOPG electrode. Further research is required to design a reagentless biosensor successfully.

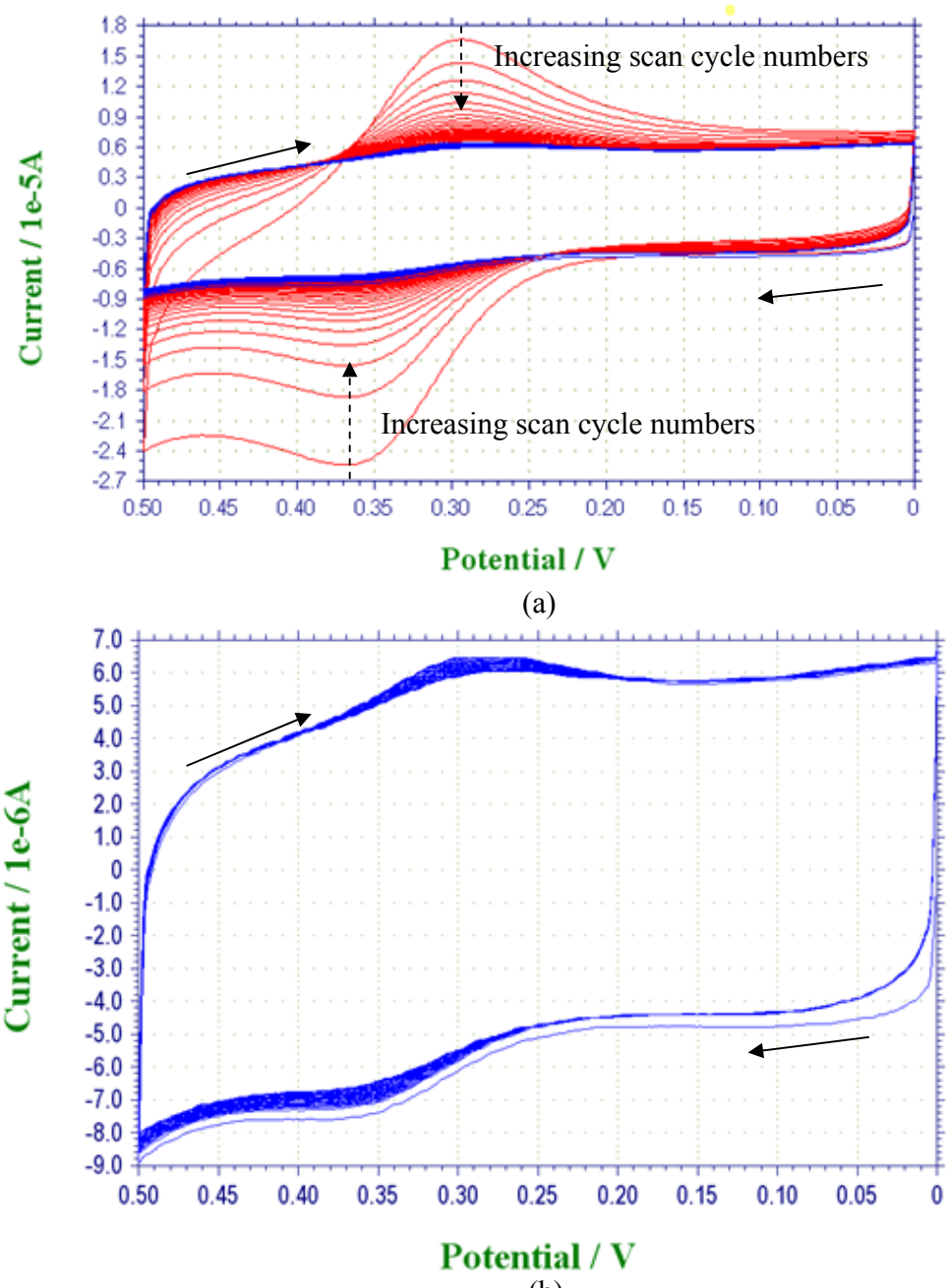

Figure 4.14 Cyclic voltammograms of HOPG/EAK16-II/FCA electrode. (a) Two consecutive sets of 25 cycles. The red line is the first set and the blue line is the second set. (b) An enlarged figured of the second set in (a). Scan rate is 50mV/s. The electrode area is 1cm×1cm. The solid arrows denote the scan direction. The dash arrows denote that the peak currents decrease as increasing scan cycle numbers.

4.3.4 Immobilization of Cytochrome *c* (Cyt *c*) onto EAK16-II Modified HOPG Electrode

The interaction and direct electron transfer between redox proteins and electrode surface are of great importance and have been widely investigated during the past few years.[49,142,143] Understanding of these reactions fundamentally can provide a desirable model for studying the redox behaviour of the proteins in biological systems, which may elucidate the relationship between their structure and biological functions.

Cytochrome *c* (Cyt *c*) is one of the well-studied redox proteins. The single iron atom in the Cyt c molecule alternates between the Fe (II) and Fe (III) oxidation states as it functions in the transport of electrons. The purpose of this section is to study the immobilization of Cyt *c* on an EAK16-II-modified electrode and the direct electron transfer. The isoeletric point of Cyt *c* is around 10.2, while that of EAK16-II is 6.3.[110] So, at pH 7, Cyt *c* is positively charged while EAK16-II is negatively charged. The electrostatic attraction between Cyt *c* and EAK16-II may enable Cyt *c* to adsorb onto the EAK16-II modified HOPG electrode.

Two electrodes were prepared and compared. The first electrode was prepared by injecting 100µl 5mM potassium phosphate buffer containing 1mg/ml Cyt *c* onto HOPG electrode and incubating at 4ºC overnight (HOPG/Cyt *c*). The second electrode was prepared by injecting 100µl 5mM potassium phosphate buffer containing 1mg/ml Cyt *c* onto EAK16-II modified HOPG electrode and incubating at 4ºC overnight (HOPG/EAK16-II/Cyt *c*). Figure 4.15 shows the cyclic voltammograms of these two electrodes. The redox peaks of Cyt *c* can be seen on both curves, which indicates that active Cyt *c* molecules have been immobilized onto both electrodes. This also indicates that there is direct electron transfer between the iron center of the protein and the electrode. The surprising aspect is that there seems to be no big difference in the redox current

between these two electrodes. The modification of the electrode with EAK16-II does not help the adsorption of Cyt *c* in this case.

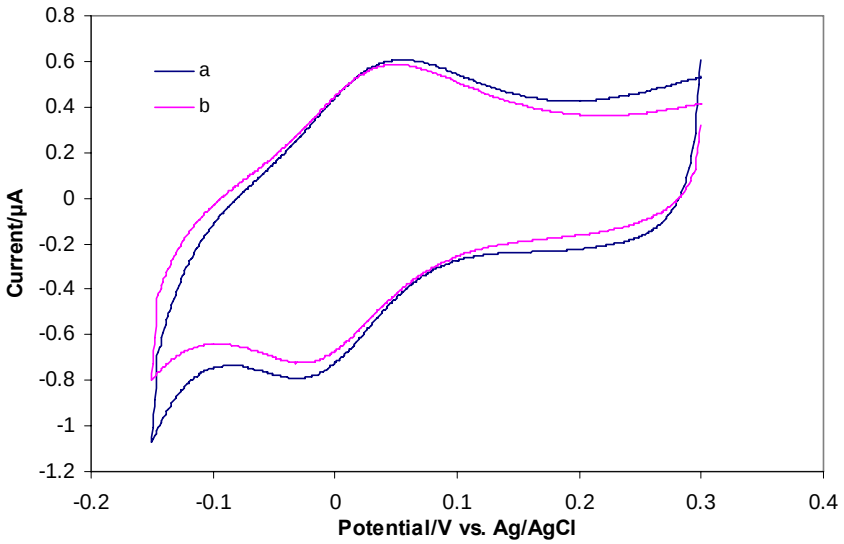

Figure 4.15 Cyclic voltammograms of HOPG/Cyt *c* (a) and HOPG/EAK16-II/Cyt *c* (b) in 5mM potassium phosphate buffer (pH 7.3). The scan rate is 2mV/s.

Similar to glucose oxidase (GOx), Cyt *c* also has amine groups on its periphery. This makes it possible to covalently immobilize Cyt *c* onto EAK16-II using the same method as for GOx. The EAK16-II modified HOPG electrode was first activated by EDC and sulfo-NHS; then 100μl 5mM potassium phosphate buffer (pH 7.3) containing 1mg/ml Cyt *c* was injected onto this electrode surface and incubated at 4ºC overnight (HOPG/EAK16-II-Cyt *c*). The cyclic voltammogram of this electrode is shown in Figure 4.16 (b). Although the redox peaks of Cyt *c* appear, the redox peak currents are almost the same as HOPG/Cyt *c*, which indicates that the immobilization of Cyt *c* is not improved in this case.

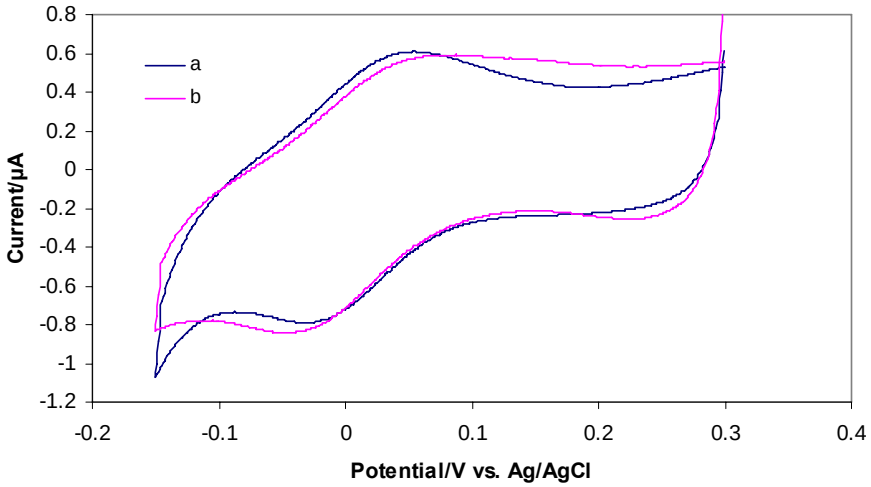

Figure 4.16 Cyclic voltammograms of HOPG/Cyt *c* (a) and HOPG/EAK16-II-Cyt *c* (b) in 5mM potassium phosphate buffer (pH 7.3). The scan rate is 2mV/s.

From theoretical analysis, the EAK16-II-modified HOPG electrode should be a useful platform for immobilization of Cyt *c*, due to the electrostatic interaction between the peptide and Cyt *c*. In addition, EAK16-II molecules are rich in functional groups for covalent bond formation between the protein and the peptide. Although this idea has not proven to be successful yet, the EAK16-II modified electrode system should be a good candidate for protein immobilization.

4.4 Conclusions

The ionic-complementary peptide EAK16-II was used to modify an HOPG electrode. Nanofibres of the self-assembling peptide formed on the electrode surface due to hydrophobic interactions between the peptide and the HOPG surface. Carboxyl groups from glutamic acid residues were used to immobilize GOx. A glucose biosensor with a sensitivity as high as 2.4mA

$M^{-1}cm^{-2}$ was obtained. The linear detection range is from 0 to 8mM glucose. An attempt has also been made to immobilize the mediator, ferrocene carboxylic acid (FCA), and a redox protein, cytochrome *c* (Cyt *c*) onto the EAK16-II modified HOPG electrode. Although these attempts were not successful in this study, the EAK16-II modified HOPG platform has potential for immobilizing various molecules or proteins.

Chapter 5 Conclusions and Recommendations

5.1 Conclusions

The ionic-complementary peptide EFK16-II was used to modify an HOPG electrode by forming a nanofibre structure of the self-assembling peptide on the electrode surface. Carboxyl groups from glutamic acid residues were used to immobilize GOx. However, we found in this study that amine groups from lysine residues of EFK16-II can also react with nearby carboxyl groups, forming intra- or interpeptide amide bonds and negatively affecting enzyme immobilization. To overcome this problem, we introduced a simple and straightforward method for GOx immobilization. A mixed solution of GOx, EDC and sulfo-NHS was injected onto the surface of EFK16-II modified HOPG electrodes. This method inhibited cross-linking of the peptide itself and more active GOx molecules were immobilized. A much higher current density (49.7μA/cm^2 vs. 9.4μA/cm^2 at 30mM glucose) and sensitivity (4.94mAM^{-1}cm^{-2} vs. 0.84mA M^{-1} cm^{-2}) were achieved with this method. The greatly enhanced electrochemical performance makes the ionic-complementary peptide modified electrode a promising platform in biosensing applications.

Another ionic-complementary peptide EAK16-II was also used to modify the HOPG electrode. Nanofibre of the sellf-assembling peptide formed on the electrode surface due to hydrophobic interactions between the peptide and the HOPG surface. Carboxyl groups from glutamic acid residues were used to immobilize GOx. A glucose biosensor with a sensitivity as high as 2.4mA M^{-1}cm^{-2} was obtained. The linear detection range is from 0 to 8mM glucose. An attempt has also been made to immobilize the mediator, ferrocene carboxylic acid (FCA), and a redox protein, cytochrome *c* (Cyt *c*) onto the EAK16-II modified HOPG electrode. Although results obtained so

far are not good enough, this EAK16-II modified HOPG platform has potential in immobilizing various molecules or proteins.

5.2 Recommendations

In order to gain further insight in the application of ionic-complementary peptide in electrode modification and biomolicular sensing, research in this area can focus on the following:

1. A model electrode, highly ordered pyrolytic graphite (HOPG) electrode, was used in this study. Further research can be conducted by using other electrode materials such as glassy carbon, gold or platinum. The self-assembly of the ionic-complementary peptide on these electrode should first be studied. Different types of morphology of peptide assembly may form on different electrode surfaces. These different types of peptide modified electrodes can be further investigated for use in enzyme or protein immobilization.

2. Most of the study in the thesis focused on the immobilization of glucose oxidase (GOx) and glucose sensing. This ionic-complementary modified electrode platform may be useful in the immobilization of other enzymes or proteins. Some recommended enzymes and proteins are: uricase, cytochrome *c*, myoglobin, hemoglobin and horseradish peroxidise.

3. Three ionic-complementary peptides were studied in the thesis, EFK16-II (Chapter 3), EAK16-II (Chapter 4) and EAR16-II (Appendix). Other ionic-complementary peptides may also be useful for biosensor applications and may have advantages in terms of sensitivity, stability, detection limit or linear detection range. A full list of the family of ionic-complementary is shown in Table 2.2. Research in this direction can be pursuited.

4. The glucose biosensor in this thesis is similar to the anode in biofuel cell. The work in biosensor can be easily extended to biofuel cell applications. Further research can focus on the application of this ionic-complementary peptide modified electrode in a biofuel cell.

Appendix

Self-assembly Study of EAR16-II and its Application in Biosensing

EAR16-II (sequence: AEAEARARAEAEARAR) is a typical ionic-complementary peptide. It has the same charge distribution pattern as EAK16-II, which is －－＋＋－－＋＋. The self-assembly of EAR16-II in aqueous solution was characterized by atomic force microscopy (AFM). Two substrates were used in this study, which were mica and highly ordered pyrolytic graphite (HOPG), respetively. The samples using these two substrates were prepared in the same way. The substrate was first cleaved so as to obtain a new and clean surface. 100μl of 100mM EAK16-II stock solution was then injected onto the freshly cleaved surface and incubated for 30min. It was then washed 3 times with Milli-Q water and was left dry for 1-2h. Silicon crystal tips (type NCL, Nanosensors^{TM}) with a radius of 10nm were used for AFM tapping mode imaging.

The AFM images of EAR16-II on mica are shown in Figure A1. Both globular and fibril structures of EAR16-II assembly are observed. The diameter of the globular structure is 160.1±19.6nm, and the height is 3.7±0.4nm; the nanofiber has a height of 1.77±0.11nm and a width of 14.19±2.75nm. On the surface of HOPG, only globular structures are observed.

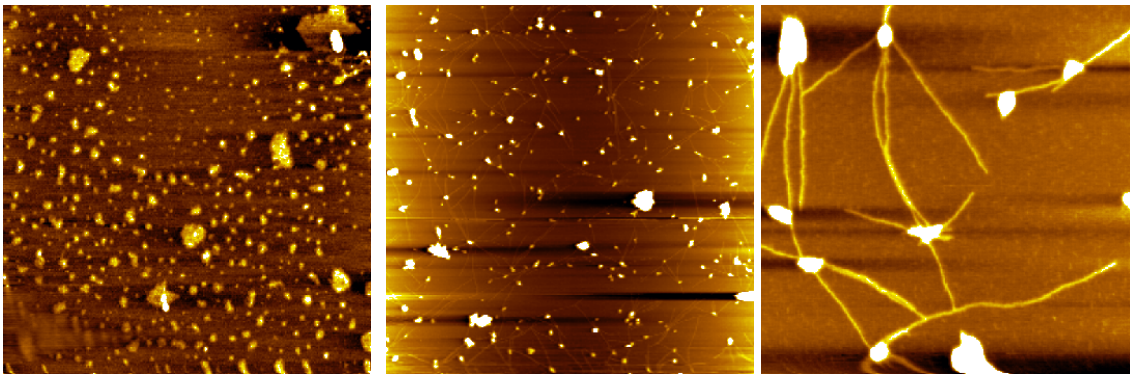

(a) (b) (c)

Figure A1 Tapping mode AFM images of EAR16-II on mica surface. The scan area of (a) and (b) is 6μm×6μm. The scan area of (c) is 1μm×1μm.

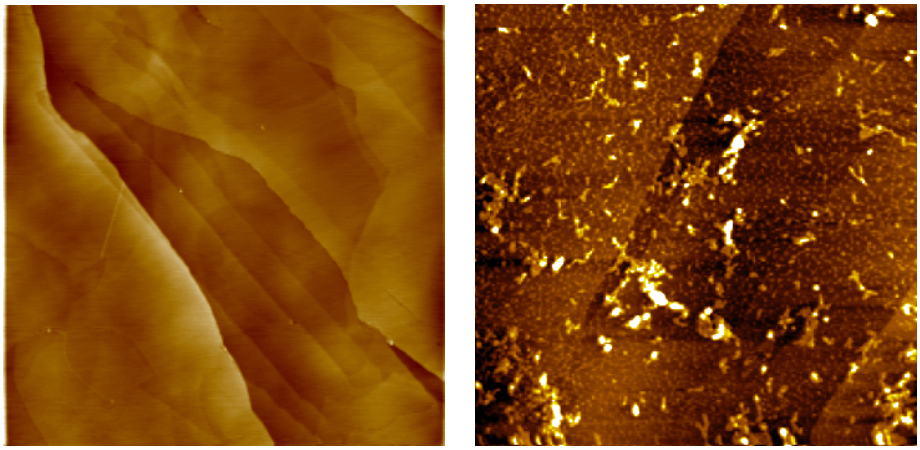

(a) (b)

Figure A2 Tapping mode AFM images of a bare HOPG surface (a) and EAR16-II modified HOPG surface. The scan area is 6μm×6μm.

EAR16-II has also been investigated in the biosensing application similar to EAK16-II and EFK16-II. 100μl 100mM EAR16-II was first injected onto a freshly cleaved HOPG electrode

surface. The electrode was then incubated at 4ºC overnight. After that, the electrode was first washed 3 times by Milli-Q water to remove loosely attached peptide. 100µl 50mM potassium phosphate (pH 5.5) containing 2mM and 5mM sulfo-NHS was then injected onto the electrode. After 1h, this electrode was washed again and 100µl 100mM potassium phosphate buffer (pH 7.0) containing 1.0mg/ml glucose was injected onto the electrode surface and incubated at 4ºC overnight (HOPG/EAR16-II/GOx). Cyclic voltammetry measurements were done using this modified electrode (HOPG/EAR16-II/GOx) as the working electrode. The result is shown in Figure A3. The anodic currents for modified electrode and unmodified electrode are almost the same, which suggests that very few active GOx molecules have been immobilized on the electrode surface. This may be because of the nanostructure of EAR16-II assembly on HOPG surface. It can be seen from Figure A2 that EAR16-II forms globular structure rather than fibril structure as EAK16-II and EFK16-II. The functional groups may be enclosed deep inside the globules so that almost no functional groups are exposed for GOx immobilization.

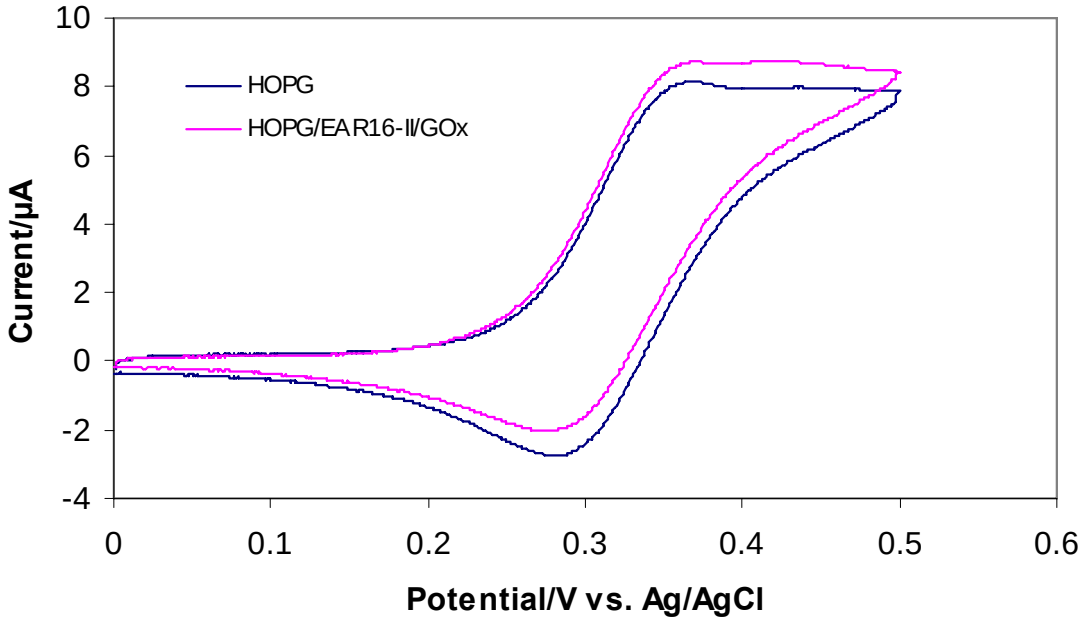

Figure A3 Cyclic voltammograms of bare HOPG electrode and HOPG/EAR16-II/GOx in 100mM potassium phosphate buffer containing 20mM glucose and 0.2mM FCA. The scan speed is 2mV/s. Electrode area is 1cm×1cm.

References

(1) Chaubey, A.; Malhotra, B. D. *Biosensors & Bioelectronics* **2002**, *17*, 441-456.

(2) Sungur, S.; Emregul, E.; Gunendi, G.; Numanoglu, Y. *Journal of Biomaterials Applications* **2004**, *18*, 265-277.

(3) Cammann, K. *Fresenius Zeitschrift Fur Analytische Chemie* **1977**, *287*, 1-9.

(4) Turner, A. P. F., Karube, I., Wilson, G.S. *Biosensors, fundamentals and applications*; Oxiford University Press: Oxford, 1987.

(5) Thevenot, D. R.; Toth, K.; Durst, R. A.; Wilson, G. S. *Biosensors & Bioelectronics* **2001**, *16*, 121-131.

(6) Crouch, E.; Cowell, D. C.; Hoskins, S.; Pittson, R. W.; Hart, J. P. *Analytical Biochemistry* **2005**, *347*, 17-23.

(7) Olaniran, A. O.; Motebejane, R. M.; Pillay, B. *Journal of Environmental Monitoring* **2008**, *10*, 889-893.

(8) Garcia-Aljaro, C.; Munoz-Berbel, X.; Munoz, F. J. *Biosensors & Bioelectronics* **2009**, *24*, 1712-1716.

(9) Hernandez, F. J.; Dondapati, S. K.; Ozalp, V. C.; Pinto, A.; O'Sullivan, C. K.; Klar, T. A.; Katakis, I. *Journal of Biophotonics* **2009**, *2*, 227-231.

(10) Sandblad, P.; Arnell, R.; Samuelsson, J.; Fornstedt, T. *Analytical Chemistry* **2009**, *81*, 3551-3559.

(11) Long, F.; He, M.; Zhu, A. N.; Shi, H. C. *Biosensors & Bioelectronics* **2009**, *24*, 2346-2351.

(12) Kim, S. J.; Gobi, K. V.; Iwasaka, H.; Tanaka, H.; Miura, N. *Biosensors & Bioelectronics* **2007**, *23*, 701-707.

(13) Salmain, M.; Fischer-Durand, N.; Pradier, C. M. *Analytical Biochemistry* **2008**, *373*, 61-70.

(14) Danielsson, B., Mosbach, K. *Biosensors: Fundamentals and Applications* **1987**, 575-595.

(15) Weaver, J. C.; Cooney, C. L.; Fulton, S. P.; Schuler, P.; Tannenbaum, S. R. *Biochimica Et Biophysica Acta* **1976**, *452*, 285-291.

(16) Sauerbrey, G. *Zeitschrift Fur Physik* **1959**, *155*, 206-222.

(17) King, W. H. *Analytical Chemistry* **1964**, *36*, 1735-1888.

(18) Shons, A.; Najarian, J.; Dorman, F. *Journal of Biomedical Materials Research* **1972**, *6*, 565-570.

(19) Abad, J. M.; Pariente, F.; Hernandez, L.; Abruna, H. D.; Lorenzo, E. *Analytical Chemistry* **1998**, *70*, 2848-2855.

(20) Minunni, M.; Skladal, P.; Mascini, M. *Analytical Letters* **1994**, *27*, 1475-1487.

(21) Cunningham, A. J. *Introduction to bioanalytial Sensors; John Wiley & Sons, Inc., New York* **1998**, 207-316.

(22) Papastathopoulos, D. S.; Rechnitz, G. A. *Analytical Chemistry* **1975**, *47*, 1792-1796.

(23) Senillou, A.; Jaffrezic-Renault, N.; Martelet, C.; Cosnier, S. *Talanta* **1999**, *50*, 219-226.

(24) Koncki, R.; Radomska, A.; Glab, S. *Talanta* **2000**, *52*, 13-17.

(25) Hahn, C. E. W. *Analyst* **1998**, *123*, 57r-86r.

(26) Clark, L. C.; Lyons, C. *Annals of the New York Academy of Sciences* **1962**, *102*, 29-45.

(27) Karyakin, A. A.; Karyakina, E. E.; Schuhmann, W.; Schmidt, H. L.; Varfolomeyev, S. D. *Electroanalysis* **1994**, *6*, 821-829.

(28) Turner, A. P. F. *Selective Electrode Reviews* **1988**, *10*, 37-38.

(29) Jaffari, S. A.; Turner, A. P. F. *Biosensors & Bioelectronics* **1997**, *12*, 1-9.

(30) Gregg, B. A.; Heller, A. *Journal of Physical Chemistry* **1991**, *95*, 5970-5975.

(31) Garjonyte, R.; Yigzaw, Y.; Meskys, R.; Malinauskas, A.; Gorton, L. *Sensors and Actuators B-Chemical* **2001**, *79*, 33-38.

(32) Wang, J. *Electroanalysis* **2001**, *13*, 983-988.

(33) Hirst, A. D.; Stevens, J. F. *Annals of Clinical Biochemistry* **1985**, *22*, 460-488.

(34) Willner, I.; Katz, E. *Angewandte Chemie-International Edition* **2000**, *39*, 1180-1218.

(35) Sarma, A. K.; Vatsyayan, P.; Goswami, P.; Minteer, S. D. *Biosensors & Bioelectronics* **2009**, *24*, 2313-2322.

(36) Babu, V. R. S.; Patra, S.; Karanth, N. G.; Kumar, M. A.; Thakur, M. S. *Analytica Chimica Acta* **2007**, *582*, 329-334.

(37) Noss, K. R.; Vaughan, A. D.; Byrne, M. E. *Journal of Applied Polymer Science* **2008**, *107*, 3435-3441.

(38) De Palma, R.; Liu, C. X.; Barbagini, F.; Reekmans, G.; Bonroy, K.; Laureyn, W.; Borghs, G.; Maes, G. *Journal of Physical Chemistry C* **2007**, *111*, 12227-12235.

(39) Wei, H. X.; Qin, Q. H.; Wen, Z. C.; Han, X. F.; Zhang, X. G. *Applied Physics Letters* **2009**, *94*, 3.

(40) Hu, P.; Huang, C. Z.; Li, Y. F.; Ling, J.; Liu, Y. L.; Fei, L. R.; Xie, J. P. *Analytical Chemistry* **2008**, *80*, 1819-1823.

(41) Cosnier, S. *Analytical Letters* **2007**, *40*, 1260-1279.

(42) Kurusu, F.; Tsunoda, H.; Saito, A.; Tomita, A.; Kadota, A.; Kayahara, N.; Karube, I.; Gotoh, M. *Analyst* **2006**, *131*, 1292-1298.

(43) Dubois, L. H.; Nuzzo, R. G. *Annual Review of Physical Chemistry* **1992**, *43*, 437-463.

(44) Bain, C. D.; Whitesides, G. M. *Angewandte Chemie-International Edition in English* **1989**, *28*, 506-512.

(45) Fenter, P.; Eberhardt, A.; Eisenberger, P. *Science* **1994**, *266*, 1216-1218.

(46) Delamarche, E.; Michel, B.; Kang, H.; Gerber, C. *Langmuir* **1994**, *10*, 4103-4108.

(47) Xia, Y. N.; Whitesides, G. M. *Angewandte Chemie-International Edition* **1998**, *37*, 551-575.

(48) Bain, C. D.; Whitesides, G. M. *Science* **1988**, *240*, 62-63.

(49) Collinson, M.; Bowden, E. F.; Tarlov, M. J. *Langmuir* **1992**, *8*, 1247-1250.

(50) Tarlov, M. J.; Bowden, E. F. *Journal of the American Chemical Society* **1991**, *113*, 1847-1849.

(51) Willit, J. L.; Bowden, E. F. *Journal of Physical Chemistry* **1990**, *94*, 8241-8246.

(52) Malem, F.; Mandler, D. *Analytical Chemistry* **1993**, *65*, 37-41.

(53) Creager, S. E.; Olsen, K. G. *Analytica Chimica Acta* **1995**, *307*, 277-289.

(54) Willner, I.; Heleg-Shabtai, V.; Blonder, R.; Katz, E.; Tao, G. L.; Buckmann, A. F.; Heller, A. *Journal of the American Chemical Society* **1996**, *118*, 10321-10322.

(55) Heller, A.; Feldman, B. *Chemical Reviews* **2008**, *108*, 2482-2505.

(56) Ling, Y.; Hammerle, M.; Olsthoorn, A. J. J.; Schuhmann, W.; Schmidt, H. L.; Duine, J. A.; Heller, A. *Analytical Chemistry* **1993**, *65*, 238-241.

(57) Mao, F.; Mano, N.; Heller, A. *Journal of the American Chemical Society* **2003**, *125*, 4951-4957.

(58) Mano, N.; Mao, F.; Heller, A. *Chemical Communications* **2004**, 2116-2117.

(59) Aoki, A.; Heller, A. *Journal of Physical Chemistry* **1993**, *97*, 11014-11019.

(60) Aoki, A.; Rajagopalan, R.; Heller, A. *Journal of Physical Chemistry* **1995**, *99*, 5102-5110.

(61) Mano, N.; Mao, F.; Heller, A. *Journal of Electroanalytical Chemistry* **2005**, *574*, 347-357.

(62) Koide, S.; Yokoyama, K. *Journal of Electroanalytical Chemistry* **1999**, *468*, 193-201.

(63) Iijima, S. *Nature* **1991**, *354*, 56-58.

(64) Schlittler, R. R.; Seo, J. W.; Gimzewski, J. K.; Durkan, C.; Saifullah, M. S. M.; Welland, M. E. *Science* **2001**, *292*, 1136-1139.

(65) Tans, S. J.; Verschueren, A. R. M.; Dekker, C. *Nature* **1998**, *393*, 49-52.

(66) Cai, C. X.; Chen, J. *Analytical Biochemistry* **2004**, *332*, 75-83.

(67) Gooding, J. J.; Wibowo, R.; Liu, J. Q.; Yang, W. R.; Losic, D.; Orbons, S.; Mearns, F. J.; Shapter, J. G.; Hibbert, D. B. *Journal of the American Chemical Society* **2003**, *125*, 9006-9007.

(68) Davis, J. J.; Coles, R. J.; Hill, H. A. O. *Journal of Electroanalytical Chemistry* **1997**, *440*, 279-282.

(69) Wang, J. X.; Li, M. X.; Shi, Z. J.; Li, N. Q.; Gu, Z. N. *Analytical Chemistry* **2002**, *74*, 1993-1997.

(70) Wang, G.; Xu, J. J.; Chen, H. Y. *Electrochemistry Communications* **2002**, *4*, 506-509.

(71) Zhao, Y. D.; Zhang, W. D.; Chen, H.; Luo, Q. M.; Li, S. F. Y. *Sensors and Actuators B-Chemical* **2002**, *87*, 168-172.

(72) Yamamoto, K.; Shi, G.; Zhou, T. S.; Xu, F.; Xu, J. M.; Kato, T.; Jin, J. Y.; Jin, L. *Analyst* **2003**, *128*, 249-254.

(73) Zhao, Y. D.; Zhang, W. D.; Chen, H.; Luo, Q. M. *Analytical Sciences* **2002**, *18*, 939-941.

(74) Patolsky, F.; Weizmann, Y.; Willner, I. *Angewandte Chemie-International Edition* **2004**, *43*, 2113-2117.

(75) Yemini, M.; Reches, M.; Rishpon, J.; Gazit, E. *Nano Letters* **2005**, *5*, 183-186.

(76) Yemini, M.; Reches, M.; Gazit, E.; Rishpon, J. *Analytical Chemistry* **2005**, *77*, 5155-5159.

(77) Reches, M.; Gazit, E. *Science* **2003**, *300*, 625-627.

(78) Song, Y. J.; Challa, S. R.; Medforth, C. J.; Qiu, Y.; Watt, R. K.; Pena, D.; Miller, J. E.; van Swol, F.; Shelnutt, J. A. *Chemical Communications* **2004**, 1044-1045.

(79) Reches, M.; Gazit, E. *Nano Letters* **2004**, *4*, 581-585.

(80) Whitesides, G. M.; Boncheva, M. *Proceedings of the National Academy of Sciences of the United States of America* **2002**, *99*, 4769-4774.

(81) Holmes, T. C.; de Lacalle, S.; Su, X.; Liu, G. S.; Rich, A.; Zhang, S. G. *Proceedings of the National Academy of Sciences of the United States of America* **2000**, *97*, 6728-6733.

(82) Marini, D. M.; Hwang, W.; Lauffenburger, D. A.; Zhang, S. G.; Kamm, R. D. *Nano Letters* **2002**, *2*, 295-299.

(83) Caplan, M. R.; Moore, P. N.; Zhang, S. G.; Kamm, R. D.; Lauffenburger, D. A. *Biomacromolecules* **2000**, *1*, 627-631.

(84) Vauthey, S.; Santoso, S.; Gong, H. Y.; Watson, N.; Zhang, S. G. *Proceedings of the National Academy of Sciences of the United States of America* **2002**, *99*, 5355-5360.

(85) Santoso, S.; Hwang, W.; Hartman, H.; Zhang, S. G. *Nano Letters* **2002**, *2*, 687-691.

(86) Hartgerink, J. D.; Beniash, E.; Stupp, S. I. *Proceedings of the National Academy of Sciences of the United States of America* **2002**, *99*, 5133-5138.

(87) Pierschbacher, M. D.; Ruoslahti, E. *Journal of Biological Chemistry* **1987**, *262*, 17294-17298.

(88) Fernandez-Lopez, S.; Kim, H. S.; Choi, E. C.; Delgado, M.; Granja, J. R.; Khasanov, A.; Kraehenbuehl, K.; Long, G.; Weinberger, D. A.; Wilcoxen, K. M.; Ghadiri, M. R. *Nature* **2001**, *412*, 452-455.

(89) Ghadiri, M. R.; Granja, J. R.; Milligan, R. A.; Mcree, D. E.; Khazanovich, N. *Nature* **1993**, *366*, 324-327.

(90) Zhang, S. G. *Biotechnology Advances* **2002**, *20*, 321-339.

(91) Caplan, M. R.; Schwartzfarb, E. M.; Zhang, S. G.; Kamm, R. D.; Lauffenburger, D. A. *Biomaterials* **2002**, *23*, 219-227.

(92) Chen, P. *Colloids and Surfaces a-Physicochemical and Engineering Aspects* **2005**, *261*, 3-24.

(93) Hong, Y. S.; Legge, R. L.; Zhang, S.; Chen, P. *Biomacromolecules* **2003**, *4*, 1433-1442.

(94) Chen, P.; Policova, Z.; Susnar, S. S.; PaceAsciak, C. R.; Demin, P. M.; Neumann, A. W. *Colloids and Surfaces a-Physicochemical and Engineering Aspects* **1996**, *114*, 99-111.

(95) Makievski, A. V.; Fainerman, V. B.; Bree, M.; Wustneck, R.; Kragel, J.; Miller, R. *Journal of Physical Chemistry B* **1998**, *102*, 417-425.

(96) Soreghan, B.; Kosmoski, J.; Glabe, C. *Journal of Biological Chemistry* **1994**, *269*, 28551-28554.

(97) Lomakin, A.; Chung, D. S.; Benedek, G. B.; Kirschner, D. A.; Teplow, D. B. *Proceedings of the National Academy of Sciences of the United States of America* **1996**, *93*, 1125-1129.

(98) Fung, S. Y.; Keyes, C.; Duhamel, J.; Chen, P. *Biophysical Journal* **2003**, *85*, 537-548.

(99) Hong, Y. S.; Lau, L. S.; Legge, R. L.; Chen, P. *Journal of Adhesion* **2004**, *80*, 913-931.

(100) Greenfie.N; Fasman, G. D. *Biochemistry* **1969**, *8*, 4108-4116.

(101) Barrow, C. J.; Zagorski, M. G. *Science* **1991**, *253*, 179-182.

(102) Arakawa, T.; Timasheff, S. N. *Biochemistry* **1984**, *23*, 5912-5923.

(103) Nandi, P. K.; Robinson, D. R. *Journal of the American Chemical Society* **1972**, *94*, 1299-1308.

(104) De la Paz, M. L.; Goldie, K.; Zurdo, J.; Lacroix, E.; Dobson, C. M.; Hoenger, A.; Serrano, L. *Proceedings of the National Academy of Sciences of the United States of America* **2002**, *99*, 16052-16057.

(105) Yoo, P. J.; Nam, K. T.; Qi, J. F.; Lee, S. K.; Park, J.; Belcher, A. M.; Hammond, P. T. *Nature Materials* **2006**, *5*, 234-240.

(106) Brown, C. L.; Aksay, I. A.; Saville, D. A.; Hecht, M. H. *Journal of the American Chemical Society* **2002**, *124*, 6846-6848.

(107) Yang, G. C.; Woodhouse, K. A.; Yip, C. M. *Journal of the American Chemical Society* **2002**, *124*, 10648-10649.

(108) Kowalewski, T.; Holtzman, D. M. *Proceedings of the National Academy of Sciences of the United States of America* **1999**, *96*, 3688-3693.

(109) Severin, N.; Okhapkin, I. M.; Khokhlov, A. R.; Rabe, J. P. *Nano Letters* **2006**, *6*, 1018-1022.

(110) Yang, H.; Fung, S. Y.; Pritzker, M.; Chen, P. *Journal of the American Chemical Society* **2007**, *129*, 12200-12210.

(111) Association, A. D. *Diabetes Care* **1994**, *17*, 81-86.

(112) Terry, L. A.; White, S. F.; Tigwell, L. J. *Journal of Agricultural and Food Chemistry* **2005**, *53*, 1309-1316.

(113) Clark, L. C.; Lyons, C. *Annals of the New York Academy of Sciences* **1962**, *102*, 29-&.

(114) Frew, J. E.; Hill, H. A. O. *Analytical Chemistry* **1987**, *59*, 933A.

(115) Rivas, G. A.; Rubianes, M. D.; Rodriguez, M. C.; Ferreyra, N. F.; Luque, G. L.; Pedano, M. L.; Miscoria, S. A.; Parrado, C. *Talanta* **2007**, *74*, 291-307.

(116) Wilson, R.; Turner, A. P. F. *Biosensors & Bioelectronics* **1992**, *7*, 165-185.

(117) Situmorang, M.; Gooding, J. J.; Hibbert, D. B.; Barnett, D. *Biosensors and Bioelectronics* **1998**, *13*, 953-962.

(118) Gregg, B. A.; Heller, A. *Analytical Chemistry* **1990**, *62*, 258-263.

(119) Gooding, J. J.; Erokhin, P.; Losic, D.; Yang, W. R.; Policarpio, V.; Liu, J. Q.; Ho, F. M.; Situmorang, M.; Hibbert, D. B.; Shapter, J. G. *Analytical Sciences* **2001**, *17*, 3-9.

(120) Yemini, M.; Xu, P.; Kaplan, D. L.; Rishpon, J. *Electroanalysis* **2006**, *18*, 2049-2054.

(121) Yang, H.; Fung, S. Y.; Sun, W.; Mikkelsen, S.; Pritzker, M.; Chen, P. *Biotechnology Progress* **2008**, *24*, 964-971.

(122) Yang, H.; Fung, S.-Y.; Pritzker, M.; Chen, P. *PLoS One* **2007**, *2*, e1325, 1-11.

(123) Xiao, Y. C.; Chung, T. S.; Chng, M. L. *Langmuir* **2004**, *20*, 8230-8238.

(124) Ramanathan, K.; Pandey, S. S.; Kumar, R.; Gulati, A.; Surya, A.; Murthy, N.; Malhotra, B. D. *Journal of Applied Polymer Science* **2000**, *78*, 662-667.

(125) Zhang, S. X.; Wang, N.; Yu, H. J.; Niu, Y. M.; Sun, C. Q. *Bioelectrochemistry* **2005**, *67*, 15-22.

(126) Szamocki, R.; Velichko, A.; Muecklich, F.; Reculusa, S.; Ravaine, S.; Neugebauer, S.; Schuhmann, W.; Hempelmann, R.; Kuhn, A. *Electrochemistry Communications* **2007**, *9*, 2121-2127.

(127) Zhang, S.; Lockshin, C.; Herbert, A.; Winter, E.; Rich, A. *EMBO Journal* **1992**, *11*, 3787-96.

(128) Zhang, S.; Holmes, T.; Lockshin, C.; Rich, A. *Proceedings of the National Academy of Sciences of the United States of America* **1993**, *90*, 3334-8.

(129) Zhang, S.; Holmes, T. C.; DiPersio, C. M.; Hynes, R. O.; Su, X.; Rich, A. *Biomaterials* **1995**, *16*, 1385-93.

(130) Kisiday, J.; Jin, M.; Kurz, B.; Hung, H.; Semino, C.; Zhang, S.; Grodzinsky, A. J. *Proceedings of the National Academy of Sciences of the United States of America* **2002**, *99*, 9996-10001.

(131) Zhang, S.; Holmes, T. C.; DiPersio, C. M.; Hynes, R. O.; Su, X.; Rich, A. *Biomaterials* **1995**, *16*, 1385-93.

(132) Davis, M. E.; Motion, J. P.; Narmoneva, D. A.; Takahashi, T.; Hakuno, D.; Kamm, R. D.; Zhang, S.; Lee, R. T. *Circulation* **2005**, *111*, 442-50.

(133) Holmes, T. C.; de Lacalle, S.; Su, X.; Liu, G.; Rich, A.; Zhang, S. *Proceedings of the National Academy of Sciences of the United States of America* **2000**, *97*, 6728-33.

(134) Schwartz, J. J.; Zhang, S. *Current Opinion in Molecular Therapeutics* **2000**, *2*, 162-167.

(135) Hawiger, J. *Current Opinion in Chemical Biology* **1999**, *3*, 89-94.

(136) Aina, O. H.; Sroka, T. C.; Chen, M. L.; Lam, K. S. *Biopolymers* **2002**, *66*, 184-99.

(137) Keyes-Baig, C.; Duhamel, J.; Fung, S.-Y.; Bezaire, J.; Chen, P. *Journal of the American Chemical Society* **2004**, *126*, 7522-7532.

(138) Fung, S. Y.; Yang, H.; Bhola, P. T.; Sadatmousavi, P.; Muzar, E.; Liu, M.; Chen, P. *Advanced Functional Material* **2009**, *19*, 74-83.

(139) Finklea, H. O.; Snider, D. A.; Fedyk, J.; Sabatani, E.; Gafni, Y.; Rubinstein, I. *Langmuir* **1993**, *9*, 3660-7.

(140) Wang, D. L.; Heller, A. *Analytical Chemistry* **1993**, *65*, 1069-1073.

(141) Ohara, T. J.; Rajagopalan, R.; Heller, A. *Analytical Chemistry* **1994**, *66*, 2451-2457.

(142) Song, S.; Clark, R. A.; Bowden, E. F.; Tarlov, M. J. *Journal of Physical Chemistry* **1993**, *97*, 6564-6572.

(143) Zhang, L.; Zhang, J.; Zhang, C. H. *Biosensors & Bioelectronics* **2009**, *24*, 2085-2090.